

On modeling the Southern Ocean Phytoplankton Functional Types

Svetlana N. Losa^{1,2}, Stephanie Dutkiewicz³, Martin Losch¹, Julia Oelker⁴, Mariana A. Soppa¹, Scarlett Trimborn¹, Hongyan Xi¹, and Astrid Bracher^{1,4}

¹Alfred Wegener Institute Helmholtz Centre for Polar and Marine Research, Bremerhaven, Germany

²Shirshov Institute of Oceanology, Russian Academy of Sciences, Moscow, Russia

³Massachusetts Institute of Technology, Cambridge, Massachusetts, USA

⁴Institute of Environmental Physics (IUP), University of Bremen, Bremen, Germany

Correspondence: Svetlana Losa (Svetlana.Losa@awi.de)

Abstract.

Phytoplankton in the Southern Ocean support important ecosystems and play a key role in the earth's carbon cycle, hence affecting climate. However, current global biogeochemical models struggle to reproduce the dynamics and co-existence of key phytoplankton functional types (PFTs) in this Ocean. Here we explore the traits important to allow three key PFTs (diatoms, coccolithophores and *Phaeocystis*) to have distributions, dominance and composition consistent with observations. In this study we use the Darwin biogeochemical/ecosystem model coupled to the Massachusetts Institute of Technology (MIT) general circulation model (Darwin-MITgcm). We evaluated our model against an extensive synthesis of observations, including *in situ* microscopy and high-performance liquid chromatography (HPLC), and satellite derived phytoplankton dominance, PFT chlorophyll-a (Chl-a), and phenology metrics. To capture the regional timing of diatom blooms obtained from satellite required including both a lightly silicified diatom type and a larger and heavy silicified type in the model. To obtain the anticipated distribution of coccolithophores, including the Great Calcite Belt, required accounting for a high affinity for nutrients and an ability to escape grazing control of this PFT. The implementation of two life stages of *Phaeocystis* to simulate both solitary and colonial forms of this PFT (with switching between forms being driven by iron availability) improved the co-existence of coccolithophores and *Phaeocystis* north of the Polar Front. The dual life-stages of *Phaeocystis* allowed it to compete both with other phytoplankton of larger size and/or similar sizes. The evaluation of simulated PFTs showed significant agreement to a large set of matchups with *in situ* PFT Chl-a data derived from pigment concentrations. Satellite data provided important qualitative comparisons of PFT phenology and PFT dominance. With these newly added traits the model produced the observed >50% coccolithophore contribution to the biomass of biomineralizing PFTs in the Great Calcite Belt. The model together with the large synthesis of observations provides a clearer picture of the Southern Ocean phytoplankton community structure, and new appreciation of the traits that are likely important in setting this structure.

1 Introduction

The Southern Ocean is one of the most important regions in regulating climate via the uptake of about 40% of the global oceanic anthropogenic CO₂ (DeVries, 2014) and at the same time, is a region with the dynamics evidently altered by past and

present climate change (Stocker et al., 2013). The climatic changes in the Southern Ocean environmental conditions affect the spatial distribution of phytoplankton (Deppeler and Davidson, 2017). The phenology and dominance of different phytoplankton functional types (PFTs) sustaining the marine food web affect the diversity of higher trophic levels (Edwards and Richardson, 2004). Playing distinct roles in biogeochemical cycling, PFTs may determine how and on which spatial and temporal scales the ocean mediates climate (Wilson et al., 2018).

Major bloom-forming PFTs in the Southern Ocean include the silicifying diatoms, calcifying coccolithophores, and colony-forming *Phaeocystis*. Diatoms, the major phytoplankton silicifiers and primary producers in the Southern Ocean (Rousseaux and Gregg, 2014), have high efficiency of carbon export through grazing, direct sinking of single cells, and through mass sedimentation events (Le Quéré et al., 2005; Kemp et al., 2006). They form large spring blooms in the open nutrient-rich waters in the proximity of the Antarctic Circumpolar Current and Polar Front (Smetacek et al., 2002; Kemp et al., 2006). Coccolithophores, the main phytoplanktonic calcifiers in the world ocean, make a major contribution to the total content of particulate inorganic carbon in the oceans (Ackleson et al., 1988; Milliman, 1993; Rost and Riebesell, 2004; Monteiro et al., 2016) through production and release of calcium carbonate plates (coccoliths), and, therefore, also impact the alkalinity of the ocean. This PFT is abundant along the Great Calcite Belt (Balch et al., 2016) and forms massive blooms along the Patagonian shelf break (Signorini et al., 2006). *Phaeocystis* as a dimethyl sulfide producer alters the atmospheric sulfur cycle and can form dense spring blooms in the seasonal ice zone and Antarctic coastal waters as the Ross Sea and Weddell Sea (El-Sayed et al., 1983; Arrigo et al., 1999; DiTullio et al., 2000; Smith et al., 2012), likely supporting export production (Arrigo et al., 2000; DiTullio et al., 2000; Wang and Moore, 2011). Modeling studies reported the contribution of diatoms to the total primary production in the Southern Ocean of ~89% (Rousseaux and Gregg, 2014), coccolithophores of ~7-16.5% (Rousseaux and Gregg, 2014; Nissen et al., 2018) and *Phaeocystis* of ~13% (*P. antarctica*) (Wang and Moore, 2011).

Despite the recognized importance of the PFTs, global biogeochemical models struggle to represent the Southern Ocean phytoplankton community accurately. The difficulties primarily originate from uncertain parameters employed in the parametrizations of, e.g., phytoplankton growth and grazing (Anderson, 2005), that define the differences in the phytoplankton traits. On the other hand, the available observational information is still limited in the Southern Ocean to allow to properly constrain the models.

One of the most investigated regions in the Southern Ocean is the Ross Sea, where many *in situ* observations on diatoms and *Phaeocystis* have been collected and inspired regional coupled ocean-sea ice-ecosystem modeling activities (Arrigo et al., 2003; Worthen and Arrigo, 2003; Kaufman et al., 2017). Several studies that include *Phaeocystis* in the list of simulated PFTs in the frame of global coupled ocean-biogeochemical models have focused on the Southern Ocean (Lancelot et al., 2009; Wang and Moore, 2011; Le Quéré et al., 2016). These studies specified differences in (photo-)physiological parameters between diatoms and *Phaeocystis*, considering *Phaeocystis* in colony form. In a regional study (Popova et al. 2007, Crozet Islands) within the Southern Ocean, *Phaeocystis* was represented by two different life-stages: colonies and solitary cells. This approach was also successfully used by Kaufman et al. (2017) to examine the influence of climatic changes on the Ross Sea phytoplankton.

Nevertheless, an in-depth evaluation of the model simulations of diatoms and *Phaeocystis* with PFT observations either has not been done (e.g. Lancelot et al. 2009) or has been only performed based on a sparse *in situ* dataset (Wang and Moore,

2011). A more complete evaluation of these PFTs was presented by Le Quéré et al. (2016) by comparing the dominance of
60 the PFTs to satellite-based dominance retrievals, and to a global dataset of *in situ*-based integrated PFT biomass within upper
200 m of Alvain et al. (2008) and (Buitenhuis et al., 2013), respectively. In general, as compared to the satellite retrievals, the
dominance of diatoms and *Phaeocystis* has been overestimated by Le Quéré et al. (2016), while dominance of coccolithophores
was underestimated.

Coccolithophore biogeography has recently been investigated globally by Monteiro et al. (2016), Krumhardt et al. (2017)
65 and Krumhardt et al. (2019), and particularly for the Southern Ocean by Nissen et al. (2018). With respect to specific coccolithophore
traits, the study by Krumhardt et al. (2017), Monteiro et al. (2016), as well as previous studies by Paasche (2001)
and Iglesias-Rodríguez et al. (2002), emphasized the high nutrient affinity of the coccolithophores and high grazing protection
of this PFT (Monteiro et al., 2016). Nissen et al. (2018) reported on higher grazing pressure on coccolithophores than on diatoms.
70 Krumhardt et al. (2019) used lower grazing pressure on coccolithophores than on diatoms and related the distribution of
coccolithophores to a specific temperature function in dependence to its growth rate. However, none of these studies included
Phaeocystis in their model simulations.

In our study, we improved the representation of key Southern Ocean PFTs, namely diatoms, coccolithophores and *Phaeocystis*,
using the Darwin biogeochemical model coupled to the Massachusetts Institute of Technology (MIT) general circulation
model (Darwin-MITgcm). In a first step, we modified the Darwin model to account for two distinct size classes of diatoms and
75 for a high affinity for nutrients and an ability to escape grazing control for coccolithophores. Next, the model was extended
to include both solitary and colonial forms of *Phaeocystis*. Observational information from *in situ* and satellite measurements
was used to help to define differences in the PFT traits, to constrain the model, as well as to quantitatively evaluate the model
performance to overall find a representation of the phytoplankton community in the Southern Ocean that is close to observations.
We used the optimized Darwin model to test three hypotheses on the factors controlling the biogeography of Southern
80 Ocean phytoplankton groups:

- Size diversity of the diatoms (Queguiner, 2013; Tréguer et al., 2018) leads to the distribution of small diatoms (“slightly
silicified and fast growing”) at the lower latitudes and large diatoms (“strongly silicified and slowly growing”) at higher
latitudes in the Southern Ocean.
- Distribution of coccolithophores in the Great Calcite Belt is not necessarily controlled by temperature (Smith et al.,
85 2017) but determined by the ability of this PFT to escape grazing because of their exoskeleton (Nejstgaard et al., 1997;
Huskin et al., 2000; Monteiro et al., 2016), and to grow under nutrient depleted conditions (especially phosphate and
iron) (Paasche, 2001; Iglesias-Rodríguez et al., 2002). These characteristics of coccolithophores would make them more
competitive among other phytoplankton of larger or similar size, small diatoms and *Phaeocystis*.
- *Phaeocystis* exists in two life stages, solitary cells and colonies, depending on iron availability (Bender et al., 2018). This
90 additional difference in the traits of distinct haptophytes, coccolithophores and *Phaeocystis*, allows them to co-exist.

The paper is organized as follows. Section 2 describes the numerical model set up, experimental design and observations (*in situ* and satellite retrievals) used for model evaluation, Section 3 presents the results and discussion. Section 4 concludes with summary and outlook.

2 Method

95 2.1 Darwin-MITgcm numerical modeling

2.1.1 Biogeochemistry

The Darwin biogeochemical model (Dutkiewicz et al., 2015) represents the ocean biogeochemical cycling of phosphorus (P), nitrogen (N), carbon (C), silicon (Si) and iron (Fe). Chlorophyll-*a* (Chl_a) and carbon are decoupled given the Geider et al. (1998) photophysiological model. The version of the Darwin model used in our study simulates, among a total
100 of 42 biogeochemical components describing these biogeochemical cycles, two types of zooplankton and six phytoplankton groups. These six (from initially nine in Dutkiewicz et al. 2015) phytoplankton groups are analogues of diatoms, nano-phytoplankton, prochlorophytes, other pico-phytoplankton (including pico-eukaryotes), nitrogen fixing phytoplankton (including *Trichodesmium*) and coccolithophores. Starting from this reduced with respect to the number of PFTs Dutkiewicz et al. (2015) Darwin configuration, the following steps have been performed to adapt the Darwin model for simulations of the South-
105 ern Ocean biogeochemistry and phytoplankton dynamics and diversity:

- Diatoms have been introduced as two distinct size classes (as two different model variables): small and “slightly silicified and fast growing” at lower latitudes (introduced instead of "other pico"); large and “strongly silicified slowly growing cells” at high latitudes (Queguiner, 2013).
- Assumed coccolithophore physiology has been accounting for high affinity for nutrients (Paasche, 2001) and ability to
110 escape grazing control (Nejstgaard et al., 1997; Huskin et al., 2000; Losa et al., 2006).
- Other nano-phytoplankton (referred to as "other large" in the original Dutkiewicz et al. 2015) has been presented by *Phaeocystis sp.*

Thus, in the modified Darwin version the following six PFTs are considered: large and small diatoms, *Phaeocystis* and coccolithophores, *Prochlorococcus*-like and N-fixers. Although later two PFTs only play a very minor role in the Southern Ocean, their
115 distributions determine the extent and abundance of small phytoplankton and coccolithophores north of the Subantarctic and Suptropical Fronts. Hence, we keep N-fixer and *Prochlorococcus*-like prokaryotes (it would also allow to maintain a reasonably good performance of the model globally). *Phaeocystis* are considered as adjusted (with respect to the traits) "other large" since "other large" did not survive in the original (Dutkiewicz et al., 2015) version that was developed for the global ocean. However, we cannot strictly state that the *Phaeocystis*-analogue considered is pure *Phaeocystis sp.*, it could be also other misrepresented
120 nano-PFTs.

In the current model configuration, instead of exploiting the radiative transfer model accounting explicitly for absorption and scattering of spectrally resolved light as in the version by Dutkiewicz et al. (2015), we use a simplified (because of computational limitations) parametrization of the light in terms of shortwave irradiance (I) penetrated over depth. Table 1 summarizes specific traits for the simulated PFTs, which are described by the following physiological parameters: the maximum photosynthetic rate (P_{max}^C , day^{-1}); the photoinhibition parameter (β) applied to *Prochlorococcus*; the growth half-saturation constant (k_{sat} , mmol m^{-3}); the biomineralizing function ($mfunc$), whether or not they form biominerals such as opal and calcite.

These main differences between specified traits alter the growth rate (μ_j , day^{-1}) of the particular phytoplankton ($j = 1, 2, \dots, 6$) and the grazing of phytoplankton by small or micro-zooplankton (Gr_{jk} , $k = 1, 2$) given the palatability factor ($r_{j,k}$) and sinking rate (w_{sink} , m day^{-1}).

The *growth* of phytoplankton is parameterized following Geider et al. (1998) to account for decoupling between Chla and C:

$$\mu_j = P_{mj}^C \left(1 - e^{-\frac{\alpha_j I \theta_j}{P_{mj}^C}}\right) \cdot f(\beta), \quad (1)$$

$$P_{mj}^C = P_{max_j}^C \gamma_T \gamma_\eta, \quad (2)$$

$$\alpha_j = \phi_{max_j} \bar{a}_j^*, \quad (3)$$

$$\gamma_\eta = \min(\eta_{lim_{ji}}, \eta_{lim_{ji}}) = \frac{\eta_i}{\eta_i + k_{sat_i}}, \quad (4)$$

$$\gamma_T = \tau_T e^{(A_T (\frac{1}{T+273.15} - \frac{1}{T_0}))} \quad (5)$$

here P_{mj}^C is the light saturated photosynthesis rate; γ_η and γ^T denote the functions of the growth rate on limiting nutrients (η_{ji} , $i = P, N, Si, Fe$) and temperature, respectively (Dutkiewicz et al., 2015); α_j is the initial slope of the photosynthesis vs. irradiance (P-I, Platt et al. 1980) curve, which is (following Dutkiewicz et al. 2015) a product of the phytoplankton-specific light absorption (considered spectrally averaged, \bar{a}_j^* , $\text{m}^2 \text{mgChla}^{-1}$) and the maximum quantum yield of carbon fixation (ϕ_{max_j} , $\text{mmolC} (\text{mol photons})^{-1}$); θ_j is the simulated chlorophyll to carbon ratio. The P_{mj}^C and k_{sat_i} parameters are specified with the use of empirical allometric relationships (Ward et al., 2012, 2017). The γ_T function was considered the same for diatom, coccolithophores, *Phaeocystis* and prokaryotes given the coefficient $\tau_T = 0.8$ normalized the maximum value (unitless), the temperature coefficient $A_T = -4000$ K, and the optimal temperature $T_0 = 293.15$ K.

Grazing is formulated as a Holling III function:

$$Gr_{jk} = g_{max_{jk}} \gamma_T \frac{r_{jk} Phy_j}{G_k} \frac{G_k^2}{G_k^2 + \kappa_{sat_k}^2}, \quad (6)$$

$$G_k = \sum_j r_{jk} Phy_j, \quad (7)$$

where $g_{max_{jk}}$ is the zooplankton maximum grazing rate on phytoplankton (d^{-1} , Dutkiewicz et al. 2015), and κ_{sat_k} is the half-saturation constant for grazing.

Sinking is expressed given the phytoplankton-specific sinking rate w_{sink_j} as:

$$Phy_{sink} = \frac{\partial w_{sink_j} Phy_j}{\partial z}. \quad (8)$$

The described biogeochemical model configuration given the parameters in Table 1 is exploited for our REF experiment. Most of the biogeochemical model parameters used in our study have been taken from the original study by Dutkiewicz et al. (2015) and from detailed laboratory studies conducted by Trimborn et al. (2017). Hence, Table 1 contains only the parameters used in the parameterizations crucial to drive the differences/diversity in the considered PFT traits. Other parameters (as well as parameterizations) not listed are the same as in Dutkiewicz et al. (2015).

In our additional experiment PHAEO, two distinct *Phaeocystis* life stages (colonies and solitary cells) have been introduced following Popova et al. (2007) and Kaufman et al. (2017). These two *Phaeocystis* life stages are considered as a function of iron availability (Bender et al., 2018): if the iron concentration is less than the iron half saturation constant (k_{satFe}), *Phaeocystis* is assumed to be present as solitary cells with the mortality rate and grazing pressure being higher by 1.3 and 1.25, respectively, than those cells in a colonial form. Following Popova et al. (2007), we consider *Phaeocystis* sinking rate (w_{sink}) dependent of available nutrients, but in our case it is limited to iron concentration as following:

$$w_{sink}(Phaeo) = w_{sink}(1 - Fe/(Fe + k_{satFe})), \quad (9)$$

$$k_{satFe}(Phaeo_{cell}) = k_{satFe}(Phaeo) * 0.8. \quad (10)$$

Note that in the model *Phaeocystis*, independent of the life stage – colonial phase or solitary cells, – is considered as one tracer. However, the assumed morphology and, therefore, physiology (mortality rate, $r_{j,k}$, k_{satFe} , sinking rate) differ as described above. We have not performed any sensitivity experiments with respect to the new parameters. However, we expect the model to be sensitive to their specification since it will also determine the competition between *Phaeocystis* and small diatoms.

2.1.2 Physics

The biogeochemical model is coupled to a global configuration of the Massachusetts Institute of Technology general circulation model (MITgcm, 2012) on a cubed-sphere grid (Adcroft et al., 2004) with a mean horizontal grid spacing of 18 km and 50 vertical levels with the resolution ranging from 10 m near the surface to 450 m in the deep ocean (Menemenlis et al., 2005; Losch et al., 2010). The simulation includes a dynamic sea-ice model with a viscous-plastic rheology and a zero-layer thermodynamic submodel (Losch et al., 2010). Penetrating light is attenuated within sea ice with an exponential law (Taylor et al. 2013, Appendix A2).

Initial conditions of the physical model were obtained from a short spin-up simulation initialised in January 1979 from rest and from temperature and salinity fields derived from the Polar Science Center Hydrographic Climatology (PHC) 3.0 (Steele et al., 2001). In the spin-up phase, the model is forced until the end of 1991 by 6-hourly atmospheric surface fields derived from the European Centre for Medium-Range Weather Forecasts (ECMWF) 40 year reanalysis (ERA-40) (Uppala et al., 2005). For more details see Losch et al. (2010, Section 3). Starting on January 1st, 1992, the model with biogeochemistry is forced until 2012 by 3-hourly atmospheric surface fields of the Japanese 55-year reanalysis (JRA55, Kobayashi et al. 2015). Initially, the model time step had to be decreased to 10 min because of the higher forcing frequency. This constraint was slowly relaxed to 20 min by January 1st, 1996. The change in forcing also required an adjustment of some of the sea-ice model parameters. The

albedos for dry ice, wet ice, dry snow, and wet snow were set to 0.75, 0.71, 0.87, and 0.81, respectively; the simulation does not use the replacement pressure method (Kimmritz et al., 2017). After spinning up the biogeochemistry for six years, during which also the physical simulation adjusts to the new forcing, the years 1999 – 2012 are integrated and the period of August 2002 – April 2012 is used for analysis.

2.1.3 Biogeochemical tracers initialisation

To initialise (in 1992) the biogeochemical model variables we use the results of the study by Taylor et al. (2013), which used a similar MITgcm configuration coupled with the Regulated Ecosystem Model (REcoM, Schartau et al. 2007) to examine the mechanisms behind the phytoplankton bloom in the Antarctic seasonal ice zone. Since their REcoM-MITgcm simulations were validated for the Southern Ocean and the variables involved in cycling N, C, Fe, Si (including inorganic and organic particular and dissolved pools) and chlorophyll-*a* (decoupled from carbon) are presented in both Darwin-MITgcm and REcoM-MITgcm models, we use correspondent REcoM-based model states as initial conditions for these variables. The model variables describing the phosphorus cycle have been initialised given N-based variables and the Redfield N:P ratio. The REcoM-based phytoplankton and zooplankton biomasses from Taylor et al. (2013) have been distributed equally between six and two Darwin PFTs and zooplankton groups, respectively.

As in previous studies using the ecosystem model (e.g. Dutkiewicz et al. 2015; Clayton et al. 2017) the plankton establishes a repeating seasonal cycle after about 3 years such that we can assume a "quasi-steady state" by year 2002. Surface nutrients are also in quasi-steady state. Longer term drift in deep nutrient distributions does not significantly change the results for the rest of the period that we consider here. It is not computationally possible to reach a totally adjusted system, and the ecological questions we address in this paper do not require such adjustments.

2.2 Evaluation with observational data

To assess our model results, we compare the simulations to several large *in situ* and satellite datasets, as detailed below and summarized in Table 2. Where the coverage of the observations is similar in respect to time we use our two-weekly model outputs. Where only monthly climatological or composite data (often from different time periods) are available we use monthly climatological model results for the period of 2006-2012. Where only results for specific months are available from observations we compare our output to these specific months. Table 3 contains the information about the evaluated phytoplankton groups as classified in the model and observations.

2.2.1 *In situ* observations

A quantitative assessment of the model has been carried out using observation from a large global and quality controlled dataset of *in situ* chlorophyll-*a* concentrations (Chl_a, mg m⁻³) of diatoms, haptophytes and prokaryotes derived from high precision liquid chromatography (HPLC) phytoplankton pigments (Soppa et al. 2017, <https://doi.pangaea.de/10.1594/PANGAEA.875879>). The dataset is composed of surface (first 12 m) measurements collected by different expeditions in the Southern

215 Ocean (south of 30°S, see Figure 1) in the time period August 2002 – April 2012, sampled mostly during austral spring and
summer months (see supplemental video materials). The phytoplankton groups for this PFT-Chla dataset were derived using
the Diagnostic Pigment Analysis (DPA) following Vidussi et al. (2001) and Uitz et al. (2006) and modified as in Hirata et al.
(2011) and Brewin et al. (2015) and adapted to a much larger dataset. Briefly, PFTs have different and specific pigments
(marker pigments, e.g. fucoxanthin – diatoms) that allow distinguishing them. The biomass of a specific PFT can be quantified
220 by determining the contribution of the corresponding diagnostic pigment to the total phytoplankton biomass (represented by
the weighted sum of the diagnostic pigments). It is worth mentioning that DPA allows also to retrieve other PFTs – like di-
noflagellates, cryptophytes and green algae – however, they were not included in this referenced dataset, originally generated
for the evaluation of satellite retrievals of diatoms, coccolithophores (haptophytes) and prokaryotes. For more details on the
method and data quality control of this *in situ* dataset, we refer the reader to the study by Losa et al. (2017, Supplementary
225 Material, Section 1 and 3).

Figure 1 shows the locations of this available *in situ* HPLC dataset in the Southern Ocean. As we can see there and in
Table 2, this large dataset gives us the possibility for a quantitative validation of our model results. Two-weekly PHAEO model
snapshots from August 2002 to April 2012 have been collocated against *in situ* HPLC-based Chla observations, if available,
within a time window ± 1 week. We compare the simulated Chla of diatoms (large + small), haptophytes (coccolithophores +
230 *Phaeocystis*) and prokaryotic pico-phytoplankton against HPLC-derived Chla for diatoms, haptophytes and prokaryotes. The
matchup statistics is presented for several biogeochemical provinces (Longhurst, 1998) distributed over the Southern Ocean
(Figure 1): Austral Polar Province (APLR), Antarctic Province (ANTA), Subantarctic Water Ring Province (SANT), South
Subtropical Convergence Province (SSTC), Humboldt Current Coastal Province (CHIL), Southwest Atlantic Shelves Province
(FKLD), Eastern Africa Coastal Province (EAFR), Australia-Indonesia Coastal Province (AUSW), East Australian Coastal
235 Province (AUSE). In the Supplementary Material we also present the distribution of the HPLC-derived Chla dataset (Soppa
et al., 2017) as seasonal climatological PFT composites.

In addition, simulations are also compared to the global MAREDAT *in situ* datasets of diatoms (Leblanc et al. 2012,
<https://doi.org/10.1594/PANGAEA.777384>), coccolithophores (O'Brien et al. 2013, <https://doi.org/10.1594/PANGAEA.785092>),
Phaeocystis spp. (Vogt et al. 2013, <https://doi.org/10.1594/PANGAEA.779101>) and micro- and mesozooplankton carbon
240 biomass (Buitenhuis et al. 2012, <https://doi.org/10.1594/PANGAEA.779970>; Moriarty et al. 2013, <https://doi.org/10.1594/PANGAEA.785501>). These datasets are based on a data collection spanning between 55 to 75 years and are provided as clima-
tological monthly composites. Because of the very sparse distribution of these datasets in the Southern Ocean (except for
zooplankton), which leads to a large representation error when comparing to the model monthly mean climatology (2006 –
2012), only a qualitative assessment was possible.

245 Predicted biomass of diatoms and coccolithophores are additionally compared to diatom and coccolithophore measurements
(as cell counts) obtained by scanning electron microscopy in the North Atlantic and Indian Ocean sections of the Southern
Ocean (the Great Calcite Belt area) during January – February 2011 and February – March 2012 by Smith et al. (2017).
For qualitative assessment of the simulated diatom and coccolithophore distributions we compare diatom *vs.* coccolithophore
dominance to similar estimates by Smith et al. (2017) collocated in space and time.

Model results of PFT dominance are compared to dominating phytoplankton groups from the monthly climatologies of the satellite product PHYSAT (1998-2006, Alvain et al. 2008). PHYSAT is based on the analysis of normalized water-leaving radiance anomalies, computed after removing the impact of chlorophyll-a variations. Specific water-leaving radiance spectra anomalies (in terms of spectral shapes and amplitudes) have been empirically associated to the presence of dominant phytoplankton groups, based on *in situ* diagnostic pigment observations. This product is based on the multispectral Sea-Viewing Wide Field-of-View Sensor (SeaWiFS) information and available in <http://log.cnrs.fr/Physat-2?lang=fr>.

We also evaluate the model simulations in terms of PFT Chla (mg m^{-3}) against the satellite PFT Chla (mg m^{-3}) product SynSenPFT (Losa et al. 2017, <https://doi.org/10.1594/PANGAEA.875873>). The SynSenPFT product combines the information of two satellite PFT Chla products: one retrieved with the differential optical absorption spectroscopy method (PhytoDOAS, Bracher et al. 2009; Sadeghi et al. 2012) applied to hyperspectral information from the Scanning Imaging Absorption Spectrometer for Atmospheric Chartography (SCIAMACHY, Bracher et al. 2017; <https://doi.org/10.1594/PANGAEA.870486>) and the OC-PFT abundance-based approach (Hirata et al. 2011 and refined in Losa et al. 2017) applied to multi-spectral satellite total Chla data from the Ocean Colour Climate Change Initiative (OC-CCI). While the PhytoDOAS products from the SCIAMACHY sensor are only available at 0.5° spatial resolution and monthly means (Bracher et al. 2017, <https://doi.org/10.1594/PANGAEA.870486>), OC-PFT applied to OC-CCI Chla products can be obtained daily and at 4 km resolution.

PhytoDOAS and PHYSAT satellite products are derived based on phytoplankton absorption properties captured by the satellite sensors and distinguished by the retrieval algorithms either as a particular PFT optical imprint ("finger print") in case of available hyperspectral information (in PhytoDOAS) or as anomalies in a multispectral signal (in PHYSAT). Thus, the PhytoDOAS allows to retrieve quantitatively major PFTs (coccolithophores, diatoms, prokaryotic phytoplankton, named in the product as cyanobacteria), while PHYSAT provides information about five dominant phytoplankton groups: prokaryotes (presented by *Prochlorococcus* and *Synechococcus*-like SCL), diatoms, haptophytes in general and *Phaeocystis* in particular.

We compare model climatology of Southern Ocean PFT dominance (averaged over the years 2006 – 2012) to the PHYSAT PFT dominance. Dominance of the modeled PFT is defined if its Chla fraction is more than 55% of the total Chla. In line with the evaluation against the PHYSAT PFT dominance, the simulated PFT dominance are compared to similar estimates obtained in the study by Dutkiewicz et al. (2015).

Two SynSenPFT products (at 4 km and daily) – diatom Chla that combines diatom Chla from PhytoDOAS and OC-PFT, and coccolithophore Chla that combines coccolithophore Chla from PhytoDOAS with haptophyte Chla from OC-PFT – are used in addition to the *in situ* based diatom vs. coccolithophores dominance by Smith et al. (2017). So we only consider the same areas and time period as in their study for comparisons of model outputs to the SynSenPFT results. Here as well the comparison is qualitative as the SynSenPFT products are mostly based on OC-PFT in our study region and the global relationships between Chla and the fraction of PFTs from the OC-PFT algorithm might differ in the Southern Ocean, as shown by Soppa et al. (2014) for diatoms.

2.3 Diatom phenological indices

285 Following Soppa et al. (2016) we evaluate the diatom phenology by calculating phenological indices based on a threshold method proposed and initially applied for assessing the TChla phenology by Siegel et al. (2002). In particular, we use the following indices: the Chla maximum date, the bloom start date, and the bloom end date. These indices are calculated based on the REF Chl simulations for diatoms (including small and large) over the year 2007/2008. We chose this particular year because: 1) with the two-weekly model output the phenological indices can be more precisely calculated than based on the
290 two-weekly or monthly mean climatology; 2) it is a typical year over the period 2006 – 2012 with respect to the simulated PFT distribution (after model reached the quasi-steady state) and climate oscillations (Soppa et al., 2016).

3 Results and Discussions

In the following, we show and discuss the results of our model simulations using the REF and the PHAEO configuration either as climatological monthly means or for representative months of the year 2007/2008, particularly focusing on the austral sum-
295 mer months or just on February 2008. Our simulation results are discussed in comparison to satellite and *in situ* observations, the former Darwin-MITgcm configuration as presented in Dutkiewicz et al. (2015), and to results obtained from other global and regional modelling efforts. In Section 3.1 we discuss our model results (focusing on REF) in respect to diatom phenology and diversity within diatoms, then in Section 3.2 the model results PHAEO are presented in respect to its differentiation of haptophytes into coccolithophores and *Phaeocystis* (Section 3.2, focusing on PHAEO). The final model setup PHAEO is eval-
300 uated quantitatively and qualitatively with different satellite and *in situ* observations in Section 3.3. Prospects and limitations of our final model setup are discussed in Section 3.4.

3.1 Diversity within diatoms

Fig. 2 depicts the PFT dominance as obtained from our REF simulations, the PHYSAT satellite observations and former Darwin-MITgcm simulations by Dutkiewicz et al. (2015). for climatological December, January, February and July. For com-
305 plete 12 monthly mean climatologies for PFT dominance as retrieved by PHYSAT and predicted in Dutkiewicz et al. (2015) and REF experiment, the reader is referred to the Supplementary Material (Figures S15 – S17, respectively). In general, the PHYSAT Southern Ocean PFT dominance climatology (over the years 1998 – 2006) shows a strong seasonal variability of PFT compositions and contributions of PFTs to TChla (Alvain et al., 2008). From November to January south of 40°S, the diatom contribution is higher than 50%. This high diatom contribution in the austral spring and summer is associated with
310 large diatom blooms starting in October at lower latitudes and moving towards higher latitudes in December – January. The nano- non-silicified phytoplankton is dominating during the time period from March to October. The Southern Ocean PFT dominance obtained in Dutkiewicz et al. (2015) disagrees with PHYSAT observations: diatoms are underrepresented in comparison to PHYSAT in circumpolar Southern Ocean during January and February, while in July they are over-represented in the Atlantic section of the Subantarctic Zone which is also opposed to the observed dominance of haptophytes. Generally, the

315 model version Dutkiewicz et al. (2015) overestimate the dominance of small non-silicified phytoplankton. These results clearly indicate deficiencies in the Dutkiewicz et al. (2015) model setup and motivated a series of Darwin-MITgcm experiments, with different model configurations with respect to assumed PFTs and their traits described by various physiological parameters. These have been conducted for the global ocean and evaluated for the Southern Ocean over the period of 2002 – 2012 with satellite observations. The detailed protocol of the experiments can be found in the Supplementary Material (Section S1).

320 Among the different experiments, the model set up REF gave the best agreement to observed phytoplankton composition, dominance and diatom phenology: This set up includes two size classes of diatoms given the parameters in Table 1, but initially without considering *Phaeocystis* in two distinct phases. Figure 2 illustrates the model phytoplankton dominance climatology obtained for the REF experiment (averaged over the period 2006 – 2012). Compared to the PHYSAT product (Figure 2 a and d), there is a significant improvement in the modeled PFT dominance using the two size classes of diatoms in relation to
325 the Darwin set up with one diatom size class as in Dutkiewicz et al. (2015) and other specific configurations as presented in the Supplementary Material (Subsections S1.1.1 – S.1.1.3). These results suggest that the too early (relative to observations) appearance of diatom blooms in the Southern Ocean simulated by most (global ocean) biogeochemical models (Vogt et al. 2013; as well in the Darwin model set up published by Dutkiewicz et al. (2015) and regional models (Nissen et al., 2018)) can be explained by the lack of inclusion of the size diversity in diatoms (Tréguer et al., 2018).

330 Figure 3 (a,b,c) shows phenological indices calculated following Soppa et al. (2016) after Siegel et al. (2002) for the REF (small+large) diatom simulations over the year 2007/2008. Looking at these figure panels along with spatial distribution of large and small diatoms (Figure 3d – f and Figure 3g – i, respectively), one can notice distinct areas of diatom bloom development: north of Polar Front with earlier bloom start date and Chla maximum date for small diatoms, and south of SACCF with later bloom start date and chlorophyll maximum date for large diatoms. The shown phenological indices agree with those presented
335 in the study by Soppa et al. (2016) and clearly indicate no phytoplankton blooms before September/October.

The augmentation of the biogeochemical module by two size classes of diatoms appeared to be a prerequisite for the simulation of the abundance of diatoms and haptophytes (including coccolithophores) in the Subantarctic Zone to be in agreement with observations (Figure 2). In order to understand how we finally reach this result of correct representation of diatoms, we have a closer look to our spring/summer 2007/2008 model REF results on small and large diatoms' biomass (presented as
340 Chla; Figure 3): While large diatoms show high biomass only close to the ice edge, which in October reaches furthest north of the SAF and then decreases towards the summer months, they are absent further north. Small diatoms are much broader distributed, but only show low concentrations (<0.2 mgChla/m³).

However, it is worth emphasizing that the simulated biomass distributions of both coccolithophores and *Phaeocystis* were very sensitive to the chosen model parameters, and small changes in the Darwin model physiological parameters led to loss of
345 either *Phaeocystis* or coccolithophores. For instance, in experiment REF after reaching a quasi-steady state, coccolithophores did not survive. It happened because there were not sufficient differences between the traits assumed for coccolithophores and “other large” (or *Phaeocystis*-analogue). As a result, it took longer for the model to get in a quasi-steady state and finally lead to just one of the haptophytes survived (taking over for another). Hence, the experiment REF represents diatoms and haptophytes

after reaching a quasi-steady state, but cannot distinguish among haptophytes. In original Darwin-2015 model (Dutkiewicz et al. 2015) “other large“ did not survive.

3.2 Differentiation among haptophytes: coccolithophores vs. *Phaeocystis*

To cope with the aforementioned problem leading to two different states either with coccolithophores or with *Phaeocystis* surviving, in experiment PHAEO we introduced additional differences between the traits of these two PFTs. In particular, we considered two distinct life stages of *Phaeocystis* (colonies and solitary cells) in which its morphological features and physiology depend on iron availability (Bender et al., 2018). To illustrate the simulated Southern Ocean phytoplankton compositions, we calculated zonally averaged ratios of individual PFT biomass to summed biomass over all simulated PFTs for the following four sectors of the Southern Ocean: the Atlantic Ocean sector (AOS, 60°W – 18°E), the Indian Ocean sector (IOS, 18°E – 120°E), the Australian sector (AST, 120°E – 180°E), and the Pacific Ocean sector (POS, 180°E – 60°W). Figure 4 presents these meridional PFT distributions of the different PFTs in February 2008 (one of the months discussed in the previous subsection, Figure 3) for experiments with and without considering *Phaeocystis* in two different life stages (referred to as PHAEO and REF, respectively). One can see that in experiment REF, “other large” (Dutkiewicz et al. 2015, in our case non-silicified nano-phytoplankton including *Phaeocystis*, but not strictly) outcompetes coccolithophores leading to too low concentrations of coccolithophores north of the Polar Front, while small diatoms exist in both experiments (however, in different percentages). In experiment PHAEO, meridional distributions of the phytoplankton composition reveal that the coccolithophores fraction gradually increases to the north of the Subantarctic Front, where they reach ~30% of the total biomass. This result is comparable to the estimates of Smith et al. (2017) obtained in AOS and IOS for late summer (January – February – March) of the years 2011 and 2012. Seasonal variations of the PHAEO phytoplankton compositions are shown in the Supplementary Material (Section S3, Figure S8). These show that the fraction of coccolithophores is higher in austral winter than in summer.

For a more precise evaluation of the PHAEO results with the study by Smith et al. (2017), we show diatom vs. coccolithophores dominance collocated in space and time with observations of Smith et al. (2017) (Figure 5). Even though our estimates have been obtained based on phytoplankton biomass (mmol C m^{-3}), but not on cell counts as in Smith et al. (2017), our results agree well to their higher concentrations and dominance of diatoms in the SBDY and SACCF, while north of the Polar Front coccolithophores become more abundant (better seen in Fig. 9). As compared with Smith et al. 2017 (their figure 2), in the Atlantic section, the dominance of simulated coccolithophores (55%) is shifted northward of the Subantarctic Front leading to underestimation of the coccolithophore dominance along the polar front and south of SAF and overestimation north of SAF.

Differences in the biomass distribution between coccolithophores, *Phaeocystis* and diatoms influence zooplankton abundance as prescribed by our model assumptions and parameterization (Figure 4, blue contour). For both experiments, REF and PHAEO, simulated zooplankton is within 0 to 20 mgC m^{-3} , which agrees with *in situ* observations reported by Moriarty and O’Brien (2013) and shown in Dutkiewicz et al. (2015) and in the Supplementary Material (Figure S14). The discussed distribution of coccolithophores have been obtained under the assumption of lower palatability function (leading to lower grazing pressure) in comparison with what is assumed for other PFTs. This contradicts the study by Nissen et al. (2018), who reported

on an increased (relative to diatoms) grazing of coccolithophores as a factor controlling the coccolithophore biogeography in the Southern Ocean. Our assumptions on low palatability factor of coccolithophores are, nevertheless, backed up by studies
385 by Nejstgaard et al. (1997), Huskin et al. (2000), Losa et al. (2006) and Monteiro et al. (2016). In the study by Losa et al. (2006) on optimised biogeochemical parameters, it was shown that coccolithophore blooms are associated with low grazing pressure. Based on laboratory experiments, Nejstgaard et al. (1997) and Huskin et al. (2000) concluded that coccolithophores (due to its "stony" structure) do not influence the microzooplankton growth. While the exact mechanisms of how this PFT uses the coccolith to protect itself against grazing is not fully understood (Monteiro et al., 2016), the ability of coccolithophores
390 to escape grazing control has "relatively well-supported evidence" (see Monteiro et al. 2016 for review). High affinity of coccolithophores for nutrients (for phosphate and iron to a larger extent than for nitrogen, Paasche 2001) makes them strongly competitive in environmental conditions with declining nutrient concentrations (Paasche, 2001; Iglesias-Rodríguez et al., 2002; Krumhardt et al., 2017), for instance under strong ocean stratification or nutrient consumption by other PFTs (see Figure 6).

Figure 6 depicts the Chla spatial distribution for diatoms, *Phaeocystis* and coccolithophores for February 2008 from PHAEO.
395 We present this particular summer month of a typical year to clearly show the patterns of the depicted distribution, which could not be very obviously seen on seasonal or climatological mean maps. One can notice co-existence of simulated PHAEO diatoms and *Phaeocystis* south of the Polar Front and the co-occurrence of diatoms and coccolithophores in the Subantarctic Zone north of the Subantarctic Front. This agrees to (Smith et al., 2017) and is supported by the PhytoDOAS PFT retrievals from SCIAMACHY hyper-spectral information within the same time frame and region in Losa et al. (2018) and Smith et al.
400 (2017).

Figure 6 presents the spatial distribution of silicon (d), dissolved iron (f) and phosphate (g) in February 2008 from PHAEO. In general, the simulated surface nutrient climatology agrees well with the World Ocean Atlas (Garcia et al., 2014) with correlation coefficient of 0.90 and 0.97 and normalised standard deviation of 1.27 and 1.13 for silicon and phosphate, respectively. The spatial distribution of silicon, dissolved iron and phosphate is discussed in line with the simulated PFT Chla biogeography.
405 The regions with high iron concentrations (in the Ross Sea, along the Western Antarctic Peninsula, around the Falkland, South Georgia and South Sandwich, Crozet and Kerquen Islands) indicate the area of *Phaeocystis* potential existence in colonial form. Thus Figure 6 shows that the simulated abundance of coccolithophores north of the Subtropical Front (STF) – where phosphate occurs in very low concentrations – is explained by the introduced high affinity of this PFT to phosphate (small half-saturation rate in γ_n function) allowing coccolithophores to grow in nutrient depleted conditions. However, in the region between the
410 Subtropical and Subantarctic Fronts the occurrence of coccolithophores is more evidently linked to low grazing pressure on this PFT due to its much lower palatability for zooplankton in comparison with small diatoms or *Phaeocystis* presented by single solitary cells. As in the study by Smith et al. (2017) reported biogeography of observed coccolithophores in the Great Calcite Belt, our simulated coccolithophore Chla is distributed in the silica-depleted area, where small diatom cells, even if they could still compete for other nutrients, have higher palatability for grazers. Coccolithophores do not compete with small
415 diatoms on silica resources and might survive due to its lower palatability factor. It could also be that in this area silica limited diatoms slowly grow allowing coccolithophores for earlier access to other (not used yet by diatoms) macronutrients and iron.

Figure 7 illustrates the importance of distinguishing among haptophytes on the carbon cycling as carbon distributed into different inorganic and organic, particulate and, consequently, dissolved pools. Shown are the particulate inorganic carbon (PIC, panel a) produced by coccolithophores (see Dutkiewicz et al. 2015, their eq. A15) and ratio of PIC to total particulate dead organic matter (POC, Dutkiewicz et al. 2015, their eq. A12), PIC:POC (panel b), for the experiments PHAEO in February 2008. Due to the improved representation of the coccolithophores and, therefore, PIC (see Balch et al. 2005) in the experiment PHAEO, the depicted PHAEO PIC:POC ratio (opposed to those in REF, Figure 7c) clearly indicates that north of the SAF the value can be from 0.4 up to 1 (on the Patagonia Shelf) which is comparable with PIC:POC export ratio presented in Balch et al. (2016), even though there is a mismatch in how POC is presented in the model and how it is measured. As in the study by Balch et al. (2016) the PIC:POC ratio is lower than 0.05 south of the Polar front.

3.3 General evaluation of experiment PHAEO

In this subchapter we present the quantitative and qualitative evaluation of our final model setup PHAEO results.

3.3.1 PHAEO PFTs compared to PHYSAT and SynSenPFT satellite observations

Figure 8 depicts the spatial distribution of PHAEO model monthly mean climatology of phytoplankton dominance obtained for July, December January and February. As for the experiment REF (Figure 2), the spatial distribution of the PFT dominance agrees with PHYSAT data product better than the spatial distribution of the model results of Dutkiewicz et al. (2015). However, the results differ from the REF dominance: in July and January, the extent of diatom dominance around the Antarctic is wider, further to the north and around the Kerguelen Islands and is less in the Atlantic Section north of SAF, showing even larger agreement to the spatial distribution of PHYSAT.

Figure 9 presents the March 2012 monthly mean spatial distribution of simulated surface Chla for coccolithophores and diatoms over the region from 30°S to 70°S and from 70°W to 120°E as shown in the study by Smith et al. (2017). These model results are compared with Chla obtained for the same domain and time with SynSenPFT algorithm (Losa et al., 2017). The simulated coccolithophore distribution reveals the calcite belt around 35°S to <50°S, which in comparison with SynSenPFT is well agreeing considering the northern boundary. The results are supported by the PhytoDOAS PFT retrievals from hyper-spectral information presented in the study by Losa et al. (2018, https://oceanopticsconference.org/extended/Losa_Svetlana.pdf) for the related region and time frame. But opposed to these satellite products the predicted calcite belt is not extending further south of the Polar Front. In this respect, it is worth emphasizing that SynSenPFT product at the latitudes higher than 60°S is mostly influenced by OC-PFT estimates because of much less available SCIAMACHY information (see Supplementary Material, Section S2) and the OC-PFT retrievals (Losa et al., 2017) contain information generally on haptophytes (not specifically on coccolithophores). Moreover, PhytoDOAS coccolithophore retrievals are based on coccolithophore specific absorption spectrum that is, indeed, very similar to the specific absorption spectrum of *Phaeocystis*. Model simulations, as seen from Figures 4 and 6, support the evidence of *Phaeocystis* dominance among haptophytes at these latitudes. Thus, SynSenPFT more likely overestimates coccolithophore Chla at the latitudes higher than 60°S. For diatoms, modeled Chla exceeds SynSenPFT estimates south of the Antarctic Circumpolar Current Front. However, SynSenPFT diatom Chla is known to be underestimated for

450 the Antarctic Province (see Losa et al. (2017)). At the same time, diatom Chla estimates obtained with PhytoDOAS are higher (see Supplementary Material, Section S2) despite the low coverage of the product, which can indicate that predicted model diatom Chla could be a bit less overestimated than it is suggested by comparison with SynSenPFT.

3.3.2 PHAEO against *in situ* HPLC-based observations

Two-weekly PHAEO model Chla snapshots for diatoms (large + small), haptophytes (coccolithophores + *Phaeocystis*) and
455 prokaryotic pico-phytoplankton over the time period from August 2002 to April 2012 were compiled as three video files, which are available as video supplement (registered via AV-Portal of the German National Library of Science and Technology - TIB: <https://doi.org/10.5446/42871>; <https://doi.org/10.5446/42873>; <https://doi.org/10.5446/42873>). The depicted snapshots are overlaid by *in situ* HPLC-derived Chla for diatom, haptophytes and prokaryotes (from Soppa et al. 2017) if available within ± 1 week. Although these videos only allow visual comparison, they do show that the *in situ* observations (indicated by
460 circles) match well the model Chla of diatoms and haptophytes in the area close to the Antarctic Peninsula and in the Southwest Atlantic Shelves biogeochemical province (FKLD, Longhurst, 1998), which illustrates a good agreement between the model and observations. In the Ross Sea, however, the model performance is less accurate: our simulated Chla for *Phaeocystis* as haptophytes in Ross Sea are underrepresented in comparison with HPLC-derived estimates. However, the comparison of *Phaeocystis* biomass to the MAREDAT dataset (Vogt et al., 2012) revealed quite a good agreement (see Section 3.3.3). The
465 total Chla agrees with OC-CCI total Chla product with a correlation coefficient $r = 0.67$ and mean absolute deviation (mean absolute error) $MAE = 0.21 \text{ mg m}^{-3}$.

We have obtained matchup statistics for the comparison of our PHAEO model results against the *in situ* HPLC-based PFT Chla observations by Soppa et al. (2017). The mean absolute deviation of collocated model and *in situ* PFT-Chla over the considered time frame (August 2002 – April 2012) and the entire Southern Ocean is 0.74 mg m^{-3} and 0.22 mg m^{-3} for
470 diatoms and haptophytes, respectively. Tables 4 and 5 present the statistics of model and *in situ* PFT-Chla comparison at several Longhurst's biogeochemical provinces (Longhurst 1998, see Figure 1). The highest disagreement was obtained for diatoms in the Atlantic Sector of the ANTA province, where the simulated diatom Chla is systematically overestimated by $\sim 0.5 \text{ mg m}^{-3}$. The best agreement with the HPLC based diatom Chla (excluding small provinces, see Figure 1) was obtained at the SSTC and SANT. For the haptophytes, the highest systematic error towards overestimation has been found at two small provinces
475 east of Africa and Australia (EAFR and AUSE) with the bias = 0.57, 0.48 (mg m^{-3}), respectively. The highest random error is (RMSE = 0.62, 0.44 mg m^{-3}) at EAFR and APLR. The lowest differences between predicted and observed haptophytes was at the FKLD, SSTC provinces where haptophytes are mostly presented by coccolithophores, and at the SANT biogeochemical province, where both coccolithophores and *Phaeocystis* co-exist. As additional information on the agreement between model and observations, Figures S9 and S10 in the Supplementary Material present frequency distributions of diatoms and haptophytes
480 Chla for the simulations and measurements as well as the frequency distribution of the model and data differences. The latter shows that statistical criteria, such as MAE and root mean squared error (RMSE) give statistical meaningful metrics with respect to “model minus *in situ* Chla data” and the evaluation does not necessarily require a logarithmic transformation, as it is often done in ocean colour product validation (Brewin et al., 2010; Losa et al., 2017).

With respect to the agreement between model and observed *in situ* Chla for prokaryotic pico-phytoplankton (Soppa et. al
485 2017) depicted in Figure S11 (Supplementary Material) one can conclude that the frequency distributions of the simulated and
observed pico-phytoplankton are different, and the frequency distribution of the differences confirms that MAE and RMSE
given absolute (Table 6) or logarithmically transformed values can hardly provide satisfactory estimates. Nevertheless, it is
worth emphasizing that the largest differences between model and observed *in situ* prokaryotic pico-phytoplankton are located
along the Antarctic Peninsula.

490 It is worth mentioning that the statistical estimates between model and observation PFT-CHla were carried out using match-
ups within ± 1 week. Moreover, the model does not explicitly represent sea-ice algae and, therefore, might work less well in
the region around the sea-ice. In this respect, we have to point out that all the statistics are presented for a qualitative assessment
of the model rather than for a quantitative estimate of model uncertainties, since the representation error (Janjić et al., 2018)
related to the differences in spatial and temporal scales considered and sampled by the model vs. observations as well as to the
495 mismatch in grouping phytoplankton (Bracher et al., 2017) are quite large.

3.3.3 PHAEO against *in situ* MAREDAT PFT biomass observations

The representation error is even larger for the comparison of PHAEO monthly mean climatology of the diatom, coccolithophores and *Phaeocystis* biomass (mgC m^{-3}) with monthly composites of *in situ* PFT biomass measurements from the MAREDAT dataset. Figure S13 shows the distribution of MAREDAT seasonal (summer and spring) composites of diatom
500 (panels a and b), coccolithophores (panels d and e) and *Phaeocystis* (panels g and h) biomass data vs. PHAEO monthly climatology matchups to MAREDAT monthly climatology for diatoms (panel c), coccolithophores (f) and *Phaeocystis* (i). Because
of the poor data coverage and large discrepancies in the represented temporal and spatial scales, differences between the model
and *in situ* data are expected to be large. As a result, correlations between model and data PFT biomass from MAREDAT
datasets are weak but significant (0.23, 0.19 and 0.54 for diatoms, coccolithophores and *Phaeocystis*, respectively). In general,
505 the model overestimates PFT-carbon biomass in comparison with the *in situ* data. At the end, showing the quantitative estimates
of the data and model agreements (MAE = -0.38,-1.03,-0.61, RMSE = 0.88,1.13,1.04 for log-transformed biomass of diatoms,
coccolithophores and *Phaeocystis*, respectively), we still make a qualitative assessment. MAREDAT measurements are not
always collocated for different PFTs, thus, it is not always possible to draw conclusions on the phytoplankton composition.
However, one can notice that diatoms, coccolithophores and *Phaeocystis* do co-exist in the areas along the Subantarctic and
510 Polar Fronts (see Figure S13, in the Supplementary Material).

3.4 Perspectives and limitations of the study

Concluding from the gained experience (including sensitivity tests) on constraining the model with available observations
which lead to our PHAEO set up, from PHAEO results and their discussion with comparable datasets from *in situ*, satellite and
modelling, we come up with the following crucial points that if addressed could further improve phytoplankton composition
515 predictions in the Southern Ocean.

Phytoplankton growth: equation (3) (ϕ_{max}). The differences in the phytoplankton growth are presented mostly by the variety of the assumed maximum photosynthesis rate ($P_{max_j}^C$) and chlorophyll to carbon ratio θ_j , resulting in slower growth of coccolithophores than for diatoms and *Phaeocystis*, which determines the simulated PFT phenology and competition. The initial slope of the P-I curve (α), opposed to the study by Hickman et al. (2010) and Dutkiewicz et al. (2015), was considered identical for all PFTs. The use of PFT specific absorption spectra (Eq. (3)) when setting up the PFT traits allows the initial slope of the P-I curve (α) being distinct for particular phytoplankton. However, an improved representation of the α parameter would also require some differences in the maximum quantum yield of carbon fixation (ϕ_{max}) specification (Hiscock et al., 2008). This would further improve the model performance (for instance, *Phaeocystis antarctica* dominance in the Ross Sea) and would probably bring the assumed $P_{max_j}^C$ values (which are currently, to some extent, overestimated) closer to measurements (Tables S5, S6 Supplementary Material, Section S4). However, the ϕ_{max} is measured given α and phytoplankton specific absorption. That means that biogeochemical models have to differentiate between the α parameter for distinct PFTs.

Phaeocystis colony formation: in this study, we use very simplistic approach to parameterize life cycle transition of *Phaeocystis* given just one model tracer. In our model this transition is triggered only by iron variability (as reported by Bender et al. 2018), but not by light availability (as previously reported by Pererzak, 1993). Since we reported on our first trial, it is worth keeping in mind that the model is expected to be sensitive to the differences we specify for the mortality and grazing rates and iron uptake for colonial and single cell stage. A careful model calibration of these parameters could further improve the model performance.

Prokaryotes: even though the *Prochlorophytes*-analogue is not present/dominant in the Southern Ocean, accounting for this pico-phytoplankton is a prerequisite for the simulation of the northern edge of coccolithophores distribution south of the STF (in the SSTC bgc province). In this respect the assumption on photoinhibition for this PFT as well as for other PFTs might need a careful revision.

Remineralization and other parameterized processes: the simulated distribution, competition and co-occurrence of the key Southern Ocean PFTs are generally discussed in terms of differentiating the PFT traits via the specification of phytoplankton growth (with different light acclimation strategies and affinities to nutrients) and palatabilities for zooplankton grazing. However, there are other processes altering the model PFT dynamics. For instance (a model based evidence, not shown), augmenting the model by CDOM affected the remineralization processes altering the nutrient distribution and therefore the spatial and temporal distribution of PFTs competing for the available resources, which indicates sensitivity of the model to the parameterization of remineralization processes. One should also think of limitations due to unresolved sea-ice algae, which might lead to overestimated diatom Chla in the marginal ice zone. of algae/sea-ice interaction.

Present-day satellite retrieval algorithms allow to detect biomass (and dominance) of some PFTs including haptophytes in general (OC-PFT, Hirata et al. 2011), coccolithophores in particular (PhytoDOAS, Sadeghi et al. 2012), diatoms and cyanobacteria/prokaryotes (OC-PFT; PhytoDOAS, Bracher et al. 2009). Though there is the mismatch between the phytoplankton group-

ing used in numerical models, satellite algorithms and *in situ* observations, the information from these different sources can be
550 considered complementary.

However, when combining or comparing models and observational information, we have to keep in mind representation errors and limitations of approaches used for deriving PFT information from *in situ* and satellite observations. Generally, a temporal and spatial scale mismatch exists between *in situ* or satellite observations and model output depending on the model discretization. *In situ* measurements in the Southern Ocean are sparse in space and time and only provide a fraction of the
555 information obtained by the model. Scientific cruises in the Southern Ocean are often carried out close to the continents/ice shelf or in regions with high phytoplankton concentration (Figure 1). Satellite observations cover larger areas frequently but only cloud- and ice-free scenes which leads to a temporal bias in the Southern Ocean, where both, sea ice and clouds occur most of the year. In addition, they are limited to only observe the first optical depth, which often limits the detection of the chlorophyll maximum. The development of algorithms for deriving PFT information requires a large *in situ* dataset with
560 homogeneous temporal and spatial distribution. The DPAs used to estimate PFTs from HPLC pigments assumes that different PFTs have different marker pigments, but it is known that they can also have pigments in common (Hirata et al., 2011). This ambiguity leads to uncertainties in the *in situ* database which is, on the one hand, needed as fundamental input for the algorithms of PFT retrievals and, on the other hand, used for direct comparison with model output here. Concerning spectral based methods applied to either *in situ* or satellite data, it is difficult to distinguish the specific absorption spectra of PFTs
565 (e.g. coccolithophores and *Phaeocystis*). These and more limitations are discussed by Sathyendranath (2014) and Bracher et al. (2017).

4 Concluding remarks and outlook

An extensive synthesis of available observational data sets on the Southern Ocean PFTs allowed us to better understand their biogeography. This information was used to infer which types should coexist in which regions, and, therefore, to constrain
570 the model. Leveraging satellite estimates and *in situ* observations allowed us to define the trait requirements for capturing phytoplankton biogeography in the Southern Ocean, and we set up a model for simulating the distribution of key Southern Ocean PFTs: diatoms, coccolithophores and *Phaeocystis*. The observed co-occurrence of two different phytoplankton groups, coccolithophores and diatoms in the Subantarctic Zone (Queguiner, 2013; Smith et al., 2017) was clearly simulated by the Darwin-MITgcm model adjusted for the Southern Ocean and in a reasonable agreement with PHYSAT, PhytoDOAS and
575 SynSenPFT satellite products.

Our results support the hypothesis that introducing two size classes of diatoms in biogeochemical models is a prerequisite to simulate the observed diatom phenology and PFT distribution in general. We have also shown that the simulated biogeography of coccolithophores is not controlled by temperature itself as reported by Smith et al. (2017), since we did not use a specific for coccolithophores temperature limitation function. It was directly explained by phosphate depleting as well as by low
580 palatability of this PFT for grazers. This confirms our second hypothesis. Nevertheless, we found that the simulation of co-occurrence of coccolithophores and *Phaeocystis* required additional model developments to account for changes in assumed

life stage of *Phaeocystis* (Popova et al., 2007; Kaufman et al., 2017) subject to iron availability (Bender et al., 2018). This parameterization of morphological shifts indeed allows for co-existence of the two types of haptophytes corroborating our third hypothesis on the dependence of *Phaeocystis sp.* life stages on iron availability. By considering two life stages of *Phaeocystis* we introduce additional differences in the traits, which along with assumed physiological parameters for coccolithophores makes coccolithophores competitive among phytoplankton of larger cell size requiring higher nutrients concentration to grow or/and among PFTs of similar size – small diatoms and *Phaeocystis* solitary cells – but of higher palatability factor to be grazed. These additional differences in the traits of distinct haptophytes, coccolithophores and *Phaeocystis* allows these groups to co-exist (e.g. along the Subantarctic and Polar fronts). However, there is still room for improvement, for instance, by specifying more precisely the differences in photophysiology and related optical imprints (Moisan and Mitchell, 2018) for *Phaeocystis* in single cell and colony phases.

The evidence that coupled ocean/biogeochemical models can capture phytoplankton specific traits in the way that it can consider different aspects of differentiation among phytoplankton groups (biogeochemical role; allometric, photophysiological and optical parameters; accounting for carbon and Chla decoupling) makes them very valuable and skilful instruments. They can combine the knowledge from *in situ* measurements and remote sensing by exploiting various PFT retrieval principles used (separately) in these observations and relate them to the environmental conditions. Further extension/progress is expected by coupling a radiative transfer model to the biogeochemical model (Gregg and Rousseaux, 2016; Dutkiewicz et al., 2018) allowing to simulate spectrally resolved water leaving radiance and therefore providing perspectives to assimilate explicitly multi- and hyper-spectral satellite information, which might improve PFT prediction.

600 5 Supplementary Material

The supplementary material contains a protocol of prior Darwin sensitivity experiments with differently prescribed phytoplankton traits (Section S1); PhytoDOAS diatoms Chla over the Great Calcite Belt (Section S2); seasonal variation of the meridional distribution of zonally averaged phytoplankton composition for four sections of the Southern Ocean (Section S3); *in situ* and laboratory measurement information on the photophysiological parameters of diatoms and *Phaeocystis* (Section S4); additional information on model evaluation against *in situ* HPLC (Soppa et al. 2017) and MAREDAT datasets (Section 5); monthly climatology of the PFT dominance obtained with PHYSAT, Darwin-15, REF and PHAEO (Section 6).

Video supplement. The following three video files are available via AV Portal of German National Library of Science and Technology (TIB, Hannover): Simulated distribution of chlorophyll-*a* concentration for diatoms (small + large) and *in situ* HPLC-derived diatom chlorophyll-*a* concentration in the Southern Ocean over the time period of August 2002 – April 2012, <https://doi.org/10.5446/42871>; Simulated distribution of chlorophyll-*a* concentration for haptophytes (coccolithophores + *Phaeocystis*) and *in situ* HPLC-derived haptophyte chlorophyll-*a* concentration in the Southern Ocean over the time period of August 2002 – April 2012, <https://doi.org/10.5446/42873>; Simulated distribution of prokaryotic pico-phytoplankton chlorophyll-*a* concentration and *in situ* HPLC-derived prokaryote chlorophyll-*a* concentration in the Southern Ocean over the time period of August 2002 – April 2012, <https://doi.org/10.5446/42872>.

Code and data availability. The model data were generated with the MIT Darwin Project Biogeochemical, Ecosystem, and Optical Model.
615 The code is part of the MITgcm, which is available from <http://mitgcm.org>. The specific version of the code used in this study, as well as initial fields can be provided upon request from the corresponding author (svetlana.losa@awi.de). Information about observational data availability is provided in the text (via specified URL).

Competing interests. The authors declare that they have no conflict of interest.

Author contributions. AB: funding and PhySyn project lead; SL: conception and design of the experiments, compilation of the first draft
620 of the manuscript and updates according critical revisions by all the co-authors; SD, ML, SL: model development and set up; SD, ST and SL: PFT traits; MS, HX: *in situ* PFT Chla data processing and interpretation; AB and JO: satellite retrievals; all co-authors: substantial participation in analysis and discussion of the results and their implications.

Acknowledgement. The authors are thankful to the MITgcm group for the MITgcm code, Anna Hickman for the previous efforts in the Darwin model developments, and all the scientists and crews involved in *in situ* HPLC data collection and analyses for providing their
625 pigment data. The authors thank Eva Alvarez for fruitful and inspiring discussions within the joint project "IPSO" ("Improving the prediction of photophysiology in the Southern Ocean by accounting for iron limitation, optical properties and spectral satellite data information"). The study was supported by the Deutsche Forschungsgemeinschaft (DFG, German Research Foundation) in the framework of the priority program 1158 "Antarctic Research with Comparative Investigations in Arctic Ice Areas" by the "PhySyn" project (Br2913/3-1); and Helmholtz Climate Initiative REKLIM (Regional Climate Change), a joint research project of the Helmholtz Association of German Research Centres
630 (HGF). The contribution of SL is partly made in the framework of the state assignment of the Federal Agency for Scientific Organizations (FASO) Russia (theme 0149-2019-0015). SD acknowledges NASA grant NNX16AR47G for funding. The model simulations were obtained with resources provided by the North-German Supercomputing Alliance (HLRN).

References

- Ackleson, S., Balch, W., and Holligan, P.: White waters of the Gulf of Maine, *Oceanography*, 1, 18–22, 1988.
- 635 Adcroft, A., Campin, J.-M., Hill, C., and Marshall, J.: Implementation of an atmosphere–ocean general circulation model on the expanded spherical cube, *Monthly Weather Review*, 132, 2845–2863, 2004.
- Alvain, S., Moulin, C., Dandonneau, Y., and Loisel, H.: Seasonal distribution and succession of dominant phytoplankton groups in the global ocean: A satellite view, *Global Biogeochemical Cycles*, 22, <https://doi.org/10.1029/2007GB003154>, 2008.
- Anderson, T. R.: Plankton functional type modelling: running before we can walk?, *Journal of Plankton Research*, 27, 1073–1081, 640 <https://doi.org/10.1093/plankt/fbi076>, <https://doi.org/10.1093/plankt/fbi076>, 2005.
- Arrigo, K. R., Robinson, D. H., Worthen, D. L., Dunbar, R. B., DiTullio, G. R., VanWoert, M., and Lizotte, M. P.: Phytoplankton Community Structure and the Drawdown of Nutrients and CO₂ in the Southern Ocean, *Science*, 283, 365–367, <https://doi.org/10.1126/science.283.5400.365>, <https://science.sciencemag.org/content/283/5400/365>, 1999.
- Arrigo, K. R., DiTullio, G. R., Dunbar, R. B., Robinson, D. H., VanWoert, M., Worthen, D. L., and Lizotte, M. P.: Phytoplankton taxonomic 645 variability in nutrient utilization and primary production in the Ross Sea, *Journal of Geophysical Research: Oceans*, 105, 8827–8846, <https://doi.org/10.1029/1998JC000289>, <https://agupubs.onlinelibrary.wiley.com/doi/abs/10.1029/1998JC000289>, 2000.
- Arrigo, K. R., Worthen, D. L., and Robinson, D. H.: A coupled ocean-ecosystem model of the Ross Sea: 2. Iron regulation of phytoplankton taxonomic variability and primary production, *Journal of Geophysical Research: Oceans*, 108, <https://doi.org/10.1029/2001JC000856>, <https://agupubs.onlinelibrary.wiley.com/doi/abs/10.1029/2001JC000856>, 2003.
- 650 Balch, W. M., Gordon, H. R., Bowler, B. C., Drapeau, D. T., and Booth, E. S.: Calcium carbonate measurements in the surface global ocean based on Moderate-Resolution Imaging Spectroradiometer data, *Journal of Geophysical Research: Oceans*, 110, <https://doi.org/10.1029/2004JC002560>, 2005.
- Balch, W. M., Bates, N. R., Lam, P. J., Twining, B. S., Rosengard, S. Z., Bowler, B. C., Drapeau, D. T., Garley, R., Lubelczyk, L. C., Mitchell, C., and Rauschenberg, S.: Factors regulating the Great Calcite Belt in the Southern Ocean and its biogeochemical significance, *Global 655 Biogeochemical Cycles*, 30, 1124–1144, <https://doi.org/10.1002/2016GB005414>, 2016.
- Bender, S. J., Moran, D. M., McIlvin, M. R., Zheng, H., McCrow, J. P., Badger, J., DiTullio, G. R., Allen, A. E., and Saito, M. A.: Colony formation in *Phaeocystis antarctica*: connecting molecular mechanisms with iron biogeochemistry, *Biogeosciences*, 15, 4923–4942, <https://doi.org/10.5194/bg-15-4923-2018>, 2018.
- Bracher, A., Vountas, M., Dinter, T., Burrows, J. P., Röttgers, R., and Peeken, I.: Quantitative observation of cyanobacteria and diatoms from 660 space using PhytoDOAS on SCIAMACHY data, *Biogeosciences*, 6, 751–764, <https://doi.org/10.5194/bg-6-751-2009>, 2009.
- Bracher, A., Bouman, H. A., Brewin, R. J. W., Bricaud, A., Brotas, V., Ciotti, A. M., Clementson, L., Devred, E., Di Cicco, A., Dutkiewicz, S., Hardman-Mountford, N. J., Hickman, A. E., Hieronymi, M., Hirata, T., Losa, S. N., Mouw, C. B., Organelli, E., Raitosos, D. E., Uitz, J., Vogt, M., and Wolanin, A.: Obtaining Phytoplankton Diversity from Ocean Color: A Scientific Roadmap for Future Development, *Frontiers in Marine Science*, 4, 55, <https://doi.org/10.3389/fmars.2017.00055>, 2017.
- 665 Bracher, A., Dinter, T., Wolanin, A., Rozanov, V. V., Losa, S., and Soppa, M. A.: Global monthly mean chlorophyll a surface concentrations from August 2002 to April 2012 for diatoms, coccolithophores and cyanobacteria from PhytoDOAS algorithm version 3.3 applied to SCIAMACHY data, link to NetCDF files in ZIP archive, <https://doi.org/10.1594/PANGAEA.870486>, <https://doi.org/10.1594/PANGAEA.870486>, in supplement to: Losa, Svetlana; Soppa, Mariana A; Dinter, Tilman; Wolanin, Aleksandra; Brewin, Robert J W; Bricaud, Annick; Oelker, Julia; Peeken, Ilka; Gentili, Bernard; Rozanov, Vladimir V; Bracher, Astrid (2017): Synergistic Exploitation of Hyper- and Multi-

- 670 Spectral Precursor Sentinel Measurements to Determine Phytoplankton Functional Types (SynSenPFT). *Frontiers in Marine Science*, 4(203), 22 pp, <https://doi.org/10.3389/fmars.2017.00203>, 2017.
- Brewin, R. J., Sathyendranath, S., Hirata, T., Lavender, S. J., Barciela, R. M., and Hardman-Mountford, N. J.: A three-component model of phytoplankton size class for the Atlantic Ocean, *Ecological Modelling*, 221, 1472–1483, <https://doi.org/10.1016/j.ecolmodel.2010.02.014>, 2010.
- 675 Brewin, R. J., Sathyendranath, S., Jackson, T., Barlow, R., Brotas, V., Airs, R., and Lamont, T.: Influence of light in the mixed-layer on the parameters of a three-component model of phytoplankton size class, *Remote Sensing of Environment*, 168, 437–450, <https://doi.org/10.1016/j.rse.2015.07.004>, 2015.
- Buitenhuis, E. T., Rivkin, R. B., Sailley, S., and Le Quéré, C.: Global distributions of microzooplankton abundance and biomass - Gridded data product (NetCDF) - Contribution to the MAREDAT World Ocean Atlas of Plankton Functional Types, <https://doi.org/10.1594/PANGAEA.779970>, <https://doi.org/10.1594/PANGAEA.779970>, 2012.
- 680 Buitenhuis, E. T., Vogt, M., Moriarty, R., Bednaršek, N., Doney, S. C., Leblanc, K., Le Quéré, C., Luo, Y.-W., O'Brien, C., O'Brien, T., Peloquin, J., Schiebel, R., and Swan, C.: MAREDAT: towards a world atlas of MARine Ecosystem DATA, *Earth System Science Data*, 5, 227–239, <https://doi.org/10.5194/essd-5-227-2013>, 2013.
- Clayton, S., Dutkiewicz, S., Jahn, O., Hill, C., Heimbach, P., and Follows, M. J.: Biogeochemical versus ecological consequences of mod-
685 eled ocean physics, *Biogeosciences*, 14, 2877–2889, <https://doi.org/10.5194/bg-14-2877-2017>, <https://www.biogeosciences.net/14/2877/2017/>, 2017.
- Deppeler, S. L. and Davidson, A. T.: Southern Ocean Phytoplankton in a Changing Climate, *Frontiers in Marine Science*, 4, 40, <https://doi.org/10.3389/fmars.2017.00040>, 2017.
- DeVries, T.: The oceanic anthropogenic CO₂ sink: Storage, air-sea fluxes, and transports over the industrial era, *Global Biogeochemical Cycles*, 28, 631–647, <https://doi.org/10.1002/2013GB004739>, <https://agupubs.onlinelibrary.wiley.com/doi/abs/10.1002/2013GB004739>, 2014.
- DiTullio, G., Grebmeier, J., Arrigo, K., Lizotte, M., Robinson, D., Leventer, A., Barry, J., VanWoert, M., and Dunbar, R.: Rapid and early export of *Phaeocystis antarctica* blooms in the Ross Sea, Antarctica, *Nature*, 404, 595, 2000.
- Dutkiewicz, S., Hickman, A. E., Jahn, O., Gregg, W. W., Mouw, C. B., and Follows, M. J.: Capturing optically important constituents and
695 properties in a marine biogeochemical and ecosystem model, *Biogeosciences*, 12, 4447–4481, <https://doi.org/10.5194/bg-12-4447-2015>, 2015.
- Dutkiewicz, S., Hickman, A. E., and Jahn, O.: Modelling ocean-colour-derived chlorophyll *a*, *Biogeosciences*, 15, 613–630, <https://doi.org/10.5194/bg-15-613-2018>, 2018.
- Edwards, M. and Richardson, A. J.: Impact of climate change on marine pelagic phenology and trophic mismatch, *Nature*, 430, 881, 2004.
- 700 El-Sayed, S. Z., Biggs, D. C., and Holm-Hansen, O.: Phytoplankton standing crop, primary productivity, and near-surface nitrogenous nutrient fields in the Ross Sea, Antarctica, *Deep Sea Research Part A. Oceanographic Research Papers*, 30, 871–886, 1983.
- Garcia, H. E., Locarnini, R. A., Boyer, T. P., Antonov, J. I., Baranova, O., Zweng, M., Reagan, J., and Johnson, D.: Dissolved Inorganic Nutrients (phosphate, nitrate, silicate), in: *World Ocean Atlas 2013 Volume 4*, edited by Levitus, S. and Mishonov, A., p. 25 pp, NOAA Atlas NESDIS 76, 2014.
- 705 Geider, R. J., MacIntyre, H. L., and Kana, T. M.: A dynamic regulatory model of phytoplanktonic acclimation to light, nutrients, and temperature, *Limnology and Oceanography*, 43, 679–694, <https://doi.org/10.4319/lo.1998.43.4.0679>, 1998.

- Gregg, W. W. and Rousseaux, C. S.: Directional and Spectral Irradiance in Ocean Models: Effects on Simulated Global Phytoplankton, Nutrients, and Primary Production, *Frontiers in Marine Science*, 3, 240, <https://doi.org/10.3389/fmars.2016.00240>, 2016.
- Group, M.: MITgcm Manual, 2012.
- 710 Hickman, A. E., Dutkiewicz, S., Williams, R. G., and Follows, M. J.: Modelling the effects of chromatic adaptation on phytoplankton community structure in the oligotrophic ocean, *Marine Ecology Progress Series*, 406, 1 – 17, <https://doi.org/10.3354/meps08588>, 2010.
- Hirata, T., Hardman-Mountford, N. J., Brewin, R. J. W., Aiken, J., Barlow, R., Suzuki, K., Isada, T., Howell, E., Hashioka, T., Noguchi-Aita, M., and Yamanaka, Y.: Synoptic relationships between surface Chlorophyll-a and diagnostic pigments specific to phytoplankton functional types, *Biogeosciences*, 8, 311–327, <https://doi.org/10.5194/bg-8-311-2011>, 2011.
- 715 Hiscock, M. R., Lance, V. P., Apprill, A. M., Bidigare, R. R., Johnson, Z. I., Mitchell, B. G., Smith, W. O., and Barber, R. T.: Photosynthetic maximum quantum yield increases are an essential component of the Southern Ocean phytoplankton response to iron, *Proceedings of the National Academy of Sciences*, 105, 4775–4780, <https://doi.org/10.1073/pnas.0705006105>, 2008.
- Huskin, I., Anadon, R., / Anadon-Marqu'es, F., and Harris, R.: Ingestion, faecal pellet and egg production rates of *Calanus helgolandicus* feeding coccolithophorid versus non-coccolithophorid diets, *J. Exp. Mar. Biol. Ecol.*, pp. 239–254, 2000.
- 720 Iglesias-Rodríguez, M. D., Brown, C. W., Doney, S. C., Kleypas, J., Kolber, D., Kolber, Z., Hayes, P. K., and Falkowski, P. G.: Representing key phytoplankton functional groups in ocean carbon cycle models: Coccolithophorids, *Global Biogeochemical Cycles*, 16, 47–1–47–20, <https://doi.org/10.1029/2001GB001454>, 2002.
- Janjić, T., Bormann, N., Bocquet, M., Carton, J. A., Cohn, S. E., Dance, S. L., Losa, S. N., Nichols, N. K., Potthast, R., Waller, J. A., and Weston, P.: On the representation error in data assimilation, *Quarterly Journal of the Royal Meteorological Society*, 144, 1257–1278, <https://doi.org/10.1002/qj.3130>, 2018.
- 725 Kaufman, D. E., Friedrichs, M. A. M., Smith Jr., W. O., Hofmann, E. E., Dinniman, M. S., and Hemmings, J. C. P.: Climate change impacts on southern Ross Sea phytoplankton composition, productivity, and export, *Journal of Geophysical Research: Oceans*, 122, 2339–2359, <https://doi.org/10.1002/2016JC012514>, 2017.
- Kemp, A. E. S., Pearce, R. B., Grigorov, I., Rance, J., Lange, C. B., Quilty, P., and Salter, I.: Production of giant marine diatoms and their export at oceanic frontal zones: Implications for Si and C flux from stratified oceans, *Global Biogeochemical Cycles*, 20, <https://doi.org/10.1029/2006GB002698>, <https://agupubs.onlinelibrary.wiley.com/doi/abs/10.1029/2006GB002698>, 2006.
- 730 Kimmritz, M., Losch, M., and Danilov, S.: A comparison of viscous-plastic sea ice solvers with and without replacement pressure, *Ocean Modelling*, 115, 59 – 69, <https://doi.org/https://doi.org/10.1016/j.ocemod.2017.05.006>, <http://www.sciencedirect.com/science/article/pii/S1463500317300690>, 2017.
- 735 Kobayashi, S., Ota, Y., Harada, Y., Ebita, A., Moriya, M., Onoda, H., Onogi, K., Kamahori, H., Kobayashi, C., Endo, H., et al.: The JRA-55 reanalysis: General specifications and basic characteristics, *Journal of the Meteorological Society of Japan. Ser. II*, 93, 5–48, 2015.
- Krumhardt, K. M., Lovenduski, N. S., Iglesias-Rodríguez, M. D., and Kleypas, J. A.: Coccolithophore growth and calcification in a changing ocean, *Progress in Oceanography*, 159, 276 – 295, <https://doi.org/https://doi.org/10.1016/j.pocean.2017.10.007>, <http://www.sciencedirect.com/science/article/pii/S0079661117302148>, 2017.
- 740 Krumhardt, K. M., Lovenduski, N. S., Long, M. C., Levy, M., Lindsay, K., Moore, J. K., and Nissen, C.: Coccolithophore Growth and Calcification in an Acidified Ocean: Insights From Community Earth System Model Simulations, *Journal of Advances in Modeling Earth Systems*, 11, 1418–1437, <https://doi.org/10.1029/2018MS001483>, <https://agupubs.onlinelibrary.wiley.com/doi/abs/10.1029/2018MS001483>, 2019.

- Lancelot, C., de Montety, A., Goosse, H., Becquevort, S., Schoemann, V., Pasquer, B., and Vancoppenolle, M.: Spatial distribution of the iron supply to phytoplankton in the Southern Ocean: a model study, *Biogeosciences*, 6, 2861–2878, <https://doi.org/10.5194/bg-6-2861-2009>, <https://www.biogeosciences.net/6/2861/2009/>, 2009.
- Le Quéré, C., Harrison, S. P., Colin Prentice, I., Buitenhuis, E. T., Aumont, O., Bopp, L., Claustre, H., Cotrim Da Cunha, L., Geider, R., Giraud, X., Klaas, C., Kohfeld, K. E., Legendre, L., Manizza, M., Platt, T., Rivkin, R. B., Sathyendranath, S., Uitz, J., Watson, A. J., and Wolf-Gladrow, D.: Ecosystem dynamics based on plankton functional types for global ocean biogeochemistry models, *Global Change Biology*, 11, 2016–2040, <https://doi.org/10.1111/j.1365-2486.2005.1004.x>, 2005.
- Le Quéré, C., Buitenhuis, E. T., Moriarty, R., Alvain, S., Aumont, O., Bopp, L., Chollet, S., Enright, C., Franklin, D. J., Geider, R. J., Harrison, S. P., Hirst, A. G., Larsen, S., Legendre, L., Platt, T., Prentice, I. C., Rivkin, R. B., Saille, S., Sathyendranath, S., Stephens, N., Vogt, M., and Vallina, S. M.: Role of zooplankton dynamics for Southern Ocean phytoplankton biomass and global biogeochemical cycles, *Biogeosciences*, 13, 4111–4133, <https://doi.org/10.5194/bg-13-4111-2016>, <https://www.biogeosciences.net/13/4111/2016/>, 2016.
- Leblanc, K., Arístegui, J., Armand, L., Assmy, P., Beker, B., Bode, A., Breton, E., Cornet, V., Gibson, J., Gosselin, M.-P., Kopczynska, E., Marshall, H., Peloquin, J., Piontkovski, S., Poulton, A. J., Quéguiner, B., Schiebel, R., Shipe, R., Stefels, J., van Leeuwe, M. A., Varela, M., Widdicombe, C., and Yallop, M.: A global diatom database – abundance, biovolume and biomass in the world ocean, *Earth System Science Data*, 4, 149–165, <https://doi.org/10.5194/essd-4-149-2012>, 2012.
- Longhurst, A.: *Ecological Geography of the Sea*, Academic press, 1998.
- Losa, S., Soppa, M. A., Dinter, T., Wolanin, A., Brewin, R. J. W., Bricaud, A., Oelker, J., Peeken, I., Gentili, B., Rozanov, V. V., and Bracher, A.: Global data sets of Chlorophyll a concentration for diatoms, coccolithophores (haptophytes) and cyanobacteria obtained from in situ observations and satellite retrievals, <https://doi.org/10.1594/PANGAEA.873210>, <https://doi.org/10.1594/PANGAEA.873210>, supplement to: Losa, S et al. (2017): Synergistic Exploitation of Hyper- and Multi-Spectral Precursor Sentinel Measurements to Determine Phytoplankton Functional Types (SynSenPFT). *Frontiers in Marine Science*, 4(203), 22 pp, <https://doi.org/10.3389/fmars.2017.00203>, 2017.
- Losa, S. N., Vézina, A., Wright, D., Lu, Y., Thompson, K., and Dowd, M.: 3D ecosystem modelling in the North Atlantic: Relative impacts of physical and biological parameterizations, *Journal of Marine Systems*, 61, 230–245, <https://doi.org/10.1016/j.jmarsys.2005.09.011>, workshop on Future Directions in Modelling Physical-Biological Interactions (WKFPBPI), 2006.
- Losa, S. N., Soppa, M. A., Dinter, T., Wolanin, A., Brewin, R. J. W., Bricaud, A., Oelker, J., Peeken, I., Gentili, B., Rozanov, V., and Bracher, A.: Synergistic Exploitation of Hyper- and Multi-Spectral Precursor Sentinel Measurements to Determine Phytoplankton Functional Types (SynSenPFT), *Frontiers in Marine Science*, 4, 203, <https://doi.org/10.3389/fmars.2017.00203>, 2017.
- Losa, S. N., Oelker, J., Soppa, M. A., Losch, M., Dutkiewicz, S., Dinter, T., Richter, A., Rozanov, V. V., Burrows, J. P., and Bracher, A.: Investigating the phytoplankton diversity in the Great Calcite Belt: perspective from modelling and satellite retrievals, in: Extended Abstract, Ocean Optics Conference XXIV, Dubrovnik (Croatia), 7 October 2018 - 12 October 2018, https://oceanopticsconference.org/extended/Losa_Svetlana.pdf, 2018.
- Losch, M., Menemenlis, D., Campin, J.-M., Heimbach, P., and Hill, C.: On the formulation of sea-ice models. Part 1: Effects of different solver implementations and parameterizations, *Ocean Modelling*, 33, 129–144, 2010.
- Menemenlis, D., Hill, C., Adcroft, A., Campin, J.-M., Cheng, B., Ciotti, B., Fukumori, I., Heimbach, P., Henze, C., Köhl, A., et al.: NASA supercomputer improves prospects for ocean climate research, *Eos, Transactions American Geophysical Union*, 86, 89–96, 2005.
- Milliman, J. D.: Production and accumulation of calcium carbonate in the ocean: Budget of a nonsteady state, *Global Biogeochemical Cycles*, 7, 927–957, <https://doi.org/10.1029/93GB02524>, 1993.

- Moisan, T. A. and Mitchell, B. G.: Modeling Net Growth of *Phaeocystis antarctica* Based on Physiological and Optical Responses to Light and Temperature Co-limitation, *Frontiers in Marine Science*, 4, 437, <https://doi.org/10.3389/fmars.2017.00437>, 2018.
- 785 Monteiro, F. M., Bach, L. T., Brownlee, C., Bown, P., Rickaby, R. E. M., Poulton, A. J., Tyrrell, T., Beaufort, L., Dutkiewicz, S., Gibbs, S., Gutowska, M. A., Lee, R., Riebesell, U., Young, J., and Ridgwell, A.: Why marine phytoplankton calcify, *Science Advances*, 2, <https://doi.org/10.1126/sciadv.1501822>, <https://advances.sciencemag.org/content/2/7/e1501822>, 2016.
- Moriarty, R. and O'Brien, T. D.: Distribution of mesozooplankton biomass in the global ocean, *Earth System Science Data*, 5, 45–55, <https://doi.org/10.5194/essd-5-45-2013>, 2013.
- 790 Moriarty, R., Buitenhuis, E. T., Le Quéré, C., and Gosselin, M.-P.: Distribution of known macrozooplankton abundance and biomass in the global ocean, *Earth System Science Data*, 5, 241–257, <https://doi.org/10.5194/essd-5-241-2013>, 2013.
- Nejstgaard, J. C., Gismervik, I., and T., S. P.: Feeding and reproduction by *Calanus finmarchicus*, and microzooplankton grazing during mesocosm blooms of diatoms and the coccolithophore *Emiliana huxleyi*, *Marine Ecology Progress Series*, 147, 197–217, <https://doi.org/10.3354/meps147197>, 1997.
- Nissen, C., Vogt, M., Münnich, M., Gruber, N., and Haumann, F. A.: Factors controlling coccolithophore biogeography in the Southern Ocean, *Biogeosciences*, 15, 6997–7024, <https://doi.org/10.5194/bg-15-6997-2018>, <https://www.biogeosciences.net/15/6997/2018/>, 2018.
- 795 O'Brien, C. J., Peloquin, J. A., Vogt, M., Heinle, M., Gruber, N., Ajani, P., Andrulleit, H., Arístegui, J., Beaufort, L., Estrada, M., Karentz, D., Kopczyńska, E., Lee, R., Poulton, A. J., Pritchard, T., and Widdicombe, C.: Global marine plankton functional type biomass distributions: coccolithophores, *Earth System Science Data*, 5, 259–276, <https://doi.org/10.5194/essd-5-259-2013>, 2013.
- Orsi, A. H. and Harris, U.: Locations of the various fronts in the Southern Ocean Australian Antarctic Data Centre – CAASM Metadata, https://data.aad.gov.au/metadata/records/southern_ocean_fronts, updated 2015, 2001.
- 800 Orsi, A. H., Whitworth, T., and Nowlin, W. D.: On the meridional extent and fronts of the Antarctic Circumpolar Current, *Deep Sea Research Part I: Oceanographic Research Papers*, 42, 641 – 673, [https://doi.org/10.1016/0967-0637\(95\)00021-W](https://doi.org/10.1016/0967-0637(95)00021-W), 1995.
- Paasche, E.: A review of the coccolithophorid *Emiliana huxleyi* (Prymnesiophyceae), with particular reference to growth, coccolith formation, and calcification-photosynthesis interactions, *Phycologia*, 40, 503–529, <https://doi.org/10.2216/i0031-8884-40-6-503.1>, 2001.
- 805 Platt, T., Gallegos, C. L., and Harrison, W. G.: Photoinhibition of photosynthesis in natural assemblages of marine phytoplankton, *J. mar. Res.*, pp. 687–701, 1980.
- Popova, E., Pollard, R., Lucas, M., Venables, H., and Anderson, T.: Real-time forecasting of ecosystem dynamics during the CROZEX experiment and the roles of light, iron, silicate, and circulation, *Deep Sea Research Part II: Topical Studies in Oceanography*, 54, 1966 – 1988, <https://doi.org/10.1016/j.dsr2.2007.06.018>, the Crozet Natural Iron Bloom and Export Experiment, 2007.
- 810 Queguiner, B.: Iron fertilization and the structure of planktonic communities in high nutrient regions of the Southern Ocean, *Deep Sea Research Part II: Topical Studies in Oceanography*, 90, 43–54, <https://doi.org/10.1016/j.dsr2.2012.07.024>, <https://hal.archives-ouvertes.fr/hal-02086574>, 2013.
- Rost, B. and Riebesell, U.: Coccolithophores and the biological pump: responses to environmental changes, in: *Coccolithophores: from molecular processes to global impact*, edited by Thiestern, H. R. and Young, J. R., pp. 99–125, Springer, Berlin, 2004.
- 815 Rousseaux, C. S. and Gregg, W. W.: Interannual Variation in Phytoplankton Primary Production at A Global Scale, *Remote Sensing*, 6, 1–19, <https://doi.org/10.3390/rs6010001>, <https://www.mdpi.com/2072-4292/6/1/1>, 2014.
- Sadeghi, A., Dinter, T., Vountas, M., Taylor, B. B., Altenburg-Soppa, M., Peeken, I., and Bracher, A.: Improvement to the PhytoDOAS method for identification of coccolithophores using hyper-spectral satellite data, *Ocean Science*, 8, 1055–1070, <https://doi.org/10.5194/os-8-1055-2012>, 2012.

- 820 Sathyendranath, S.: Phytoplankton functional types from Space, in: Reports of the International Ocean-Colour Coordinating Group (IOCCG), vol. 15, pp. 1–156, International Ocean-Colour Coordinating Group, 2014.
- Schartau, M., Engel, A., Schröter, J., Thoms, S., Völker, C., and Wolf-Gladrow, D.: Modelling carbon overconsumption and the formation of extracellular particulate organic carbon, *Biogeosciences*, 4, 433–454, <https://doi.org/10.5194/bg-4-433-2007>, 2007.
- Siegel, D. A., Doney, S. C., and Yoder, J. A.: The North Atlantic Spring Phytoplankton Bloom and Sverdrup's Critical Depth Hypothesis, *Science*, 296, 730–733, <https://doi.org/10.1126/science.1069174>, 2002.
- 825 Signorini, S. R., Garcia, V. M. T., Piola, A. R., Garcia, C. A. E., Mata, M. M., and McClain, C. R.: Seasonal and interannual variability of calcite in the vicinity of the Patagonian shelf break (38°S–52°S), *Geophysical Research Letters*, 33, <https://doi.org/10.1029/2006GL026592>, 2006.
- Smetacek, V., Klaas, C., Menden-Deuer, S., and Rynearson, T. A.: Mesoscale distribution of dominant diatom species relative to the hydrographical field along the Antarctic Polar Front, *Deep Sea Research Part II: Topical Studies in Oceanography*, 49, 3835–3848, 2002.
- 830 Smith, H. E. K., Poulton, A. J., Garley, R., Hopkins, J., Lubelczyk, L. C., Drapeau, D. T., Rauschenberg, S., Twining, B. S., Bates, N. R., and Balch, W. M.: The influence of environmental variability on the biogeography of coccolithophores and diatoms in the Great Calcite Belt, *Biogeosciences*, 14, 4905–4925, <https://doi.org/10.5194/bg-14-4905-2017>, 2017.
- Smith, W. O., Gloucester, P., Sedwick, P. N., Arrigo, K. R., Ainley, D. G., and Orsi, A. H.: The Ross Sea in a Sea of Change, *Oceanography*, 835 25, <https://doi.org/10.5670/oceanog.2012.80>, 2012.
- Soppa, M. A., Hirata, T., Silva, B., Dinter, T., Peeken, I., Wiegmann, S., and Bracher, A.: Global Retrieval of Diatom Abundance Based on Phytoplankton Pigments and Satellite Data, *Remote Sensing*, 6, 10 089–10 106, <https://doi.org/10.3390/rs61010089>, 2014.
- Soppa, M. A., Völker, C., and Bracher, A.: Diatom Phenology in the Southern Ocean: Mean Patterns, Trends and the Role of Climate Oscillations, *Remote Sensing*, 8, <https://doi.org/10.3390/rs8050420>, 2016.
- 840 Soppa, M. A., Peeken, I., and Bracher, A.: Global chlorophyll a concentrations for diatoms, haptophytes and prokaryotes obtained with the Diagnostic Pigment Analysis of HPLC data compiled from several databases and individual cruises, <https://doi.org/10.1594/PANGAEA.875879>, <https://doi.org/10.1594/PANGAEA.875879>, in supplement to: Losa, Svetlana; Soppa, Mariana A; Dinter, Tilman; Wolanin, Aleksandra; Brewin, Robert J W; Bricaud, Annick; Oelker, Julia; Peeken, Ilka; Gentili, Bernard; Rozanov, Vladimir V; Bracher, Astrid (2017): Synergistic Exploitation of Hyper- and Multi-Spectral Precursor Sentinel Measurements to Determine
- 845 Phytoplankton Functional Types (SynSenPFT). *Frontiers in Marine Science*, 4(203), 22 pp, <https://doi.org/10.3389/fmars.2017.00203>, 2017.
- Steele, M., Morley, R., and Ermold, W.: PHC: A Global Ocean Hydrography with a High-Quality Arctic Ocean, *Journal of Climate*, 14, 2079–2087, [https://doi.org/10.1175/1520-0442\(2001\)014<2079:PAGOHW>2.0.CO;2](https://doi.org/10.1175/1520-0442(2001)014<2079:PAGOHW>2.0.CO;2), 2001.
- Stocker, T., Qin, D., Plattner, G.-K., Tignor, M., Allen, S., Boschung, J., Nauels, A., Xia, Y., Bex, V., and Midgley, P. e.: Climate change 2013: the physical science basis: Working Group I contribution to the Fifth assessment report of the Intergovernmental Panel on Climate Change, Cambridge University Press, Cambridge, United Kingdom and New York, NY, USA, <https://doi.org/doi:10.1017/CBO9781107415324>, 2013.
- 850 Taylor, M. H., Losch, M., and Bracher, A.: On the drivers of phytoplankton blooms in the Antarctic marginal ice zone: A modeling approach, *Journal of Geophysical Research: Oceans*, 118, 63–75, <https://doi.org/10.1029/2012JC008418>, 2013.
- 855 Trimborn, S., Thoms, S., Brenneis, T., Heiden, J. P., Beszteri, S., and Bischof, K.: Two Southern Ocean diatoms are more sensitive to ocean acidification and changes in irradiance than the prymnesiophyte *Phaeocystis antarctica*, *Physiologia Plantarum*, 160, 155–170, <https://doi.org/10.1111/ppl.12539>, <https://onlinelibrary.wiley.com/doi/abs/10.1111/ppl.12539>, 2017.

- Tréguer, P., Bowler, C., Moriceau, B., Dutkiewicz, S., Gehlen, M., Aumont, O., Bittner, L., Dugdale, R., Finkel, Z., Iudicone, D., Jahn, O., Guidi, L., Lasbleiz, M., Leblanc, K., Levy, M., and Pondaven, P.: Influence of diatom diversity on the ocean biological carbon pump, *Nature Geoscience*, 11, 27 – 37, <https://doi.org/10.1038/s41561-017-0028-x>, 2018.
- 860 Uitz, J., Claustre, H., Morel, A., and Hooker, S. B.: Vertical distribution of phytoplankton communities in open ocean: An assessment based on surface chlorophyll, *Journal of Geophysical Research: Oceans*, 111, <https://doi.org/10.1029/2005JC003207>, 2006.
- Uppala, S. M., Kållberg, P., Simmons, A., Andrae, U., Bechtold, V. D. C., Fiorino, M., Gibson, J., Haseler, J., Hernandez, A., Kelly, G., et al.: The ERA-40 re-analysis, *Quarterly Journal of the Royal Meteorological Society: A journal of the atmospheric sciences, applied meteorology and physical oceanography*, 131, 2961–3012, 2005.
- 865 Vidussi, F., Claustre, H., Manca, B. B., Luchetta, A., and Marty, J.-C.: Phytoplankton pigment distribution in relation to upper thermocline circulation in the eastern Mediterranean Sea during winter, *Journal of Geophysical Research: Oceans*, 106, 19 939–19 956, <https://doi.org/10.1029/1999JC000308>, 2001.
- Vogt, M., O'Brien, C., Peloquin, J., Schoemann, V., Breton, E., Estrada, M., Gibson, J., Karentz, D., Van Leeuwe, M. A., Stefels, J., Widdicombe, C., and Peperzak, L.: Global marine plankton functional type biomass distributions: *Phaeocystis* spp., *Earth System Science Data*, 4, 107–120, <https://doi.org/10.5194/essd-4-107-2012>, 2012.
- 870 Vogt, M., Hashioka, T., Payne, M. R., Buitenhuis, E. T., Quéré, C. L., Alvain, S., Aita, M. N., Bopp, L., Doney, S. C., Hirata, T., Lima, I., Saille, S., and Yamanaka, Y.: The distribution, dominance patterns and ecological niches of plankton functional types in Dynamic Green Ocean Models and satellite estimates, *Biogeosciences Discussions*, 10, 17 193–17 247, <https://doi.org/10.5194/bgd-10-17193-2013>, <https://www.biogeosciences-discuss.net/10/17193/2013/>, 2013.
- 875 Wang, S. and Moore, J. K.: Incorporating *Phaeocystis* into a Southern Ocean ecosystem model, *Journal of Geophysical Research: Oceans*, 116, <https://doi.org/10.1029/2009JC005817>, <https://agupubs.onlinelibrary.wiley.com/doi/abs/10.1029/2009JC005817>, 2011.
- Ward, B. A., Dutkiewicz, S., Jahn, O., and Follows, M. J.: A size-structured food-web model for the global ocean, *Limnology and Oceanography*, 57, 1877–1891, <https://doi.org/10.4319/lo.2012.57.6.1877>, 2012.
- 880 Ward, B. A., Marañón, E., Sauterey, B., Rault, J., and Claessen, D.: The Size Dependence of Phytoplankton Growth Rates: A Trade-Off between Nutrient Uptake and Metabolism, *The American Naturalist*, 189, 170–177, <https://doi.org/10.1086/689992>, PMID: 28107051, 2017.
- Wilson, J. D., Monteiro, F. M., Schmidt, D. N., Ward, B. A., and Ridgwell, A.: Linking Marine Plankton Ecosystems and Climate: A New Modeling Approach to the Warm Early Eocene Climate, *Paleoceanography and Paleoclimatology*, 33, 1439–1452, <https://doi.org/10.1029/2018PA003374>, <https://agupubs.onlinelibrary.wiley.com/doi/abs/10.1029/2018PA003374>, 2018.
- 885 Worthen, D. L. and Arrigo, K. R.: A coupled ocean-ecosystem model of the Ross Sea. Part 1: Interannual variability of primary production and phytoplankton community structure, *Biogeochemistry of the Ross Sea. Antarct Res Ser*, 78, 93–105, 2003.

Table 1. Biogeochemical model internal parameters/trait settings with *Phaeo* for *Phaeocystis*, *Prochlor* for *Prochlorococcus*, Nfixer for nitrogen fixing PFT and coccolith for coccolithophores.

Param	Units\PFTs	large diatoms	<i>Phaeo</i>	small diatoms	<i>Prochlor</i>	Nfixer	coccolith
P_{max}^C	day ⁻¹	1.79	1.59	2.16	1.09	0.31	1.23
β	unitless				1.25		
k_{sat_N}	mmol m ⁻³	0.451	0.106	0.053	0.007	0.0	0.086
k_{sat_P}	mmol m ⁻³	0.028	0.007	0.003	0.0004	0.004	0.0054
$k_{sat_{Fe}}$	μ mol m ⁻³	0.028	0.007	0.0033	0.0005	0.0124	0.0054
$k_{sat_{Si}}$	mmol m ⁻³	0.45		0.06			
$r_{j,k=1}$	unitless	0.8	0.78	0.2	0.2	0.6	0.58
$r_{j,k=2}$	unitless	0.16	0.156	1.0	1.0	0.12	0.12
w_{sink}	m day ⁻¹	0.77	0.23	0.10	0.03	0	0.23
ϕ_{max_j}	mmolC (mol photons) ⁻¹	40	40	40	40	40	40
$\overline{a_j^*}$	m ² mgChla ⁻¹	0.02	0.02	0.02	0.02	0.02	0.02
m_{pj}	day ⁻¹	0.04	0.05	0.1	0.1	0.1	0.05
$mfunc$		silicified		silicified			calcifier

P_{max}^C is the maximum photosynthetic rate at 30°C; β is the photoinhibition parameter, applied to *Prochlorococcus*; k_{sat} is the growth half-saturation constant; $r_{j,k}$ denotes the palatability factor of the particular phytoplankton ($j = 1, 2, \dots, 6$), grazing of phytoplankton for small or micro-zooplanktons ($k = 1, 2$); w_{sink} is the sinking rate; ϕ_{max_j} is the maximum quantum yield of carbon fixation; $\overline{a_j^*}$ is the spectrally averaged phytoplankton-specific light absorption; m_{pj} is the mortality rate; $mfunc$ determines the biomineralizing function.

Table 2. Datasets used for model evaluation

Dataset	reference	PFT product	units	spatial repr.	time repr.	model output	time repr.
PHYSAT	Alvain et al. (2008)	dominance	unitless	1°x1°	monthly climat. (1998-2006)	dominance	2006–2012**
Darwin-15	Dutkiewicz et al. (2015)	dominance	unitless	1°x1°	monthly climatology	dominance	2006–2012**
SEM	Smith et al. (2017)	dia vs. cocco dominance	% cell counts	in situ	Jan–Feb 2011 Feb–March 2012	dia vs. cocco % C-biomass	Jan–Feb 2011 Feb–Mar 2012
SynSenPFT	Losa et al. (2017)	diatom-Chla cocco-Chla	mgChla m ⁻³ mgChla m ⁻³	4x4 km* 4x4 km*	March 2012 March 2012	diatom-Chla cocco-Chla	March 2012 March 2012
PhytoDOAS	Bracher et al. (2017)	diatom-Chla	mgChla m ⁻³	0.5°x0.5°*	March 2012	diatom-Chla	March 2012
HPLC	Soppa et al. (2017)	diatom-Chla hapto-Chla proka-Chla	mgChla m ⁻³ mgChla m ⁻³ mgChla m ⁻³	in situ in situ in situ	Aug2002 – Apr2012 Aug2002 – Apr2012 Aug2002 – Apr2012	diatom-Chla hapto-Chla <i>Proch</i> -Chla	collocated collocated collocated
MAREDAT	Leblanc et al. (2012)	diatom-C	mgC m ⁻³	in situ	1933–2009 climat.	diatom-C	2006–2012**
	O’Brien et al. (2013)	cocco-C	mgC m ⁻³	in situ	1929–2008 climat.	cocco-C	2006–2012**
	Vogt et al. (2013)	<i>Phaeo</i> -C	mgC m ⁻³	in situ	1955–2009 climat.	<i>Phaeo</i> -C	2006–2012**
	Buitenhuis et al. (2012)	micro-zoo-C	mgC m ⁻³	in situ	climatology	zoo-C	2006–2012**
	Moriarty et al. (2013)	mezo-zoo-C	mgC m ⁻³	in situ	climatology	zoo-C	2006–2012**

diatom – Chla denotes diatom Chla; *cocco – Chla* is coccolithophore Chla; *hapto – Chla* is haptophytes Chla; *proka – Chla* is prokaryotes Chla, *Phaeo – Chla* is *Phaeocystis* Chla; *Proch – Chla* is *Prochlorococcus* Chla, extension –C denotes carbon biomass; dia vs. cocco is diatom vs. coccolithophores; zoo stands for zooplankton; repr. is representation; climat. is climatology.

* the data are presented for a reduced Southern Ocean area as in Smith et al. (2017) and Losa et al. (2018).

** model monthly mean climatology over the years 2006 – 2012.

Table 3. Table of specification of the key phytoplankton groups (PG) given their biomineralizing function (BF) and size class as referred in the observations (phytoplankton size class, PSC) and model (phytoplankton size class model, SCM).

PG	PSC	SCM	BF
Diatoms	micro/nano	"large"/"small"	silicified
large cells	micro	"large"	strongly silicified
small cells	nano	"small euk"	lightly silicified
Haptophytes	nano/pico	"other large"	
<i>Phaeocystis</i>	nano/pico	"other large"	
coccolithophores	nano	"large"	calcifier
Prokaryotes	pico		
N-fixer	pico	small	
<i>Prochlorococcus</i>	pico	"other small"	

pico < 2 μm ; 2 μm < nano < 20 μm ; micro > 20 μm

Table 4. Validation of modeled diatom Chla (mgChla m^{-3}) against *in situ* diatom Chla (mgChla m^{-3}), collocated in space and time over the time period August 2002 – April 2012, at Longhurst’s provinces.

criteria\biomes	APLR	ANTA	SANT	SSTC	CHIL	FKLD	EAFR	AUSW	AUSE
MAE (mgChla m^{-3})	1.00	0.75	0.27	0.08	0.27	0.15	0.21	0.01	0.03
RMSE (mgChla m^{-3})	1.90	1.44	0.41	0.13	0.42	0.21	0.42	0.02	0.05
RMSE unbiased	1.88	1.34	0.39	0.13	0.35	0.18	0.40	0.02	0.05
bias (mgChla m^{-3})	-0.29	0.52	-0.12	0	-0.22	-0.11	-0.13	0	0
N	1287	235	402	102	24	12	6	7	19

MAE – mean absolute error (mgChla m^{-3}); RMSE — root mean squared error (mgChla m^{-3}); biomes are the Longhurst’s biogeochemical provinces (Longhurst, 1998): Austral Polar Province (APLR), Antarctic Province (ANTA), Subantarctic Water Ring Province (SANT), South Subtropical Convergence Province (SSTC), Humboldt Current Coastal Province (CHIL), Southwest Atlantic Shelves Province (FKLD), Eastern Africa Coastal Province (EAFR), Australia-Indonesia Coastal Province (AUSW), East Australian Coastal Province (AUSE).

Table 5. Same as Table 4 but for haptophytes.

criteria\biomes	APLR	ANTA	SANT	SSTC	CHIL	FKLD	EAFR	AUSW	AUSE
MAE (mgChla m ⁻³)	0.24	0.22	0.16	0.14	0.19	0.13	0.57	0.10	0.48
RMSE (mgChla m ⁻³)	0.45	0.27	0.21	0.25	0.24	0.18	0.85	0.15	0.53
RMSE unbiased	0.44	0.26	0.21	0.26	0.22	0.17	0.62	0.12	0.22
bias (mgChla m ⁻³)	0.01	0.01	-0.10	-0.03	-0.08	-0.07	0.57	0.09	0.48
N	1264	229	437	154	26	12	12	23	39

Table 6. Same as Table 4 but for prokaryotes.

criteria \ biomes	APLR	ANTA	SANT	SSTC	CHIL	FKLD	EAFR	AUSW	AUSE
MAE (mgChla m ⁻³)	0.28	0.11	0.06	0.14	0.08	0.06	0.05	0.07	0.05
RMSE(mgChla m ⁻³)	0.64	0.19	0.13	0.22	0.13	0.08	0.05	0.08	0.05
RMSE unbiased	0.57	0.16	0.12	0.18	0.13	0.06	0.05	0.04	0.05
bias (mgChla m ⁻³)	-0.23	-0.11	-0.06	-0.13	0	-0.06	-0.02	-0.06	-0.01
N	772	42	201	82	21	7	12	39	27

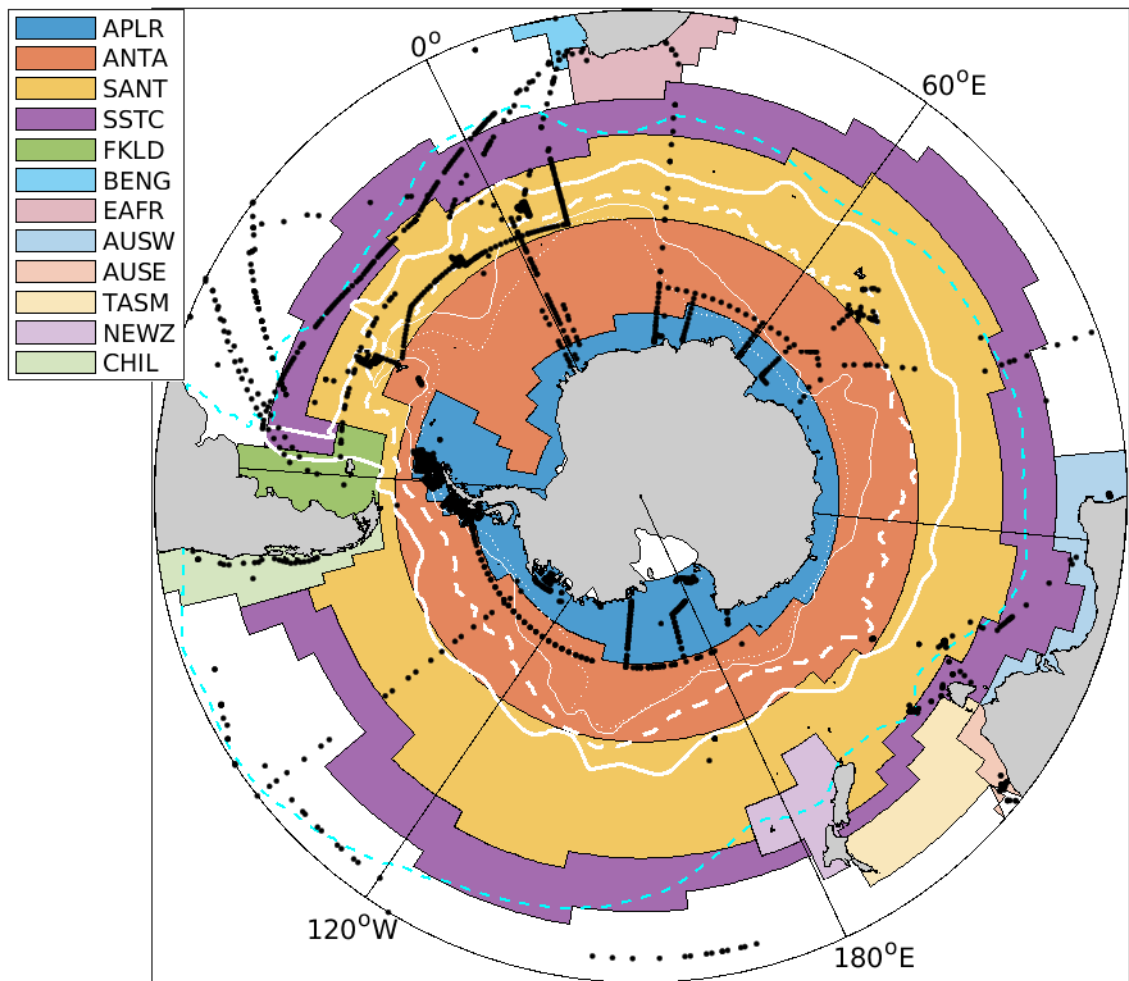


Figure 1. Distribution of *in situ* PFT-Chla observations (Soppa et al., 2017) derived from HPLC phytoplankton pigments (black dots) over the Southern Ocean at the Longhurst's biogeochemical provinces (coloured domains): Austral Polar Province (APLR), Antarctic Province (ANTA), Subantarctic Water Ring Province (SANT), South Subtropical Convergence Province (SSTC), Humboldt Current Coastal Province (CHIL), Southwest Atlantic Shelves Province (FKLD), Eastern Africa Coastal Province (EAFR), Australia-Indonesia Coastal Province (AUSW), East Australian Coastal Province (AUSE). The white contours denote the Southern Ocean fronts (Orsi et al., 1995; Orsi and Harris, 2001): the Sub-Antarctic Front (SAF, thick contour); the Polar Front (PF, dashed), the Southern Antarctic Circumpolar Current Front (SACCF, thin contour) and the Southern Boundary of ACC (SBDY, dotted). The cyan dashed contour shows the Sub-Tropical Front (STF).

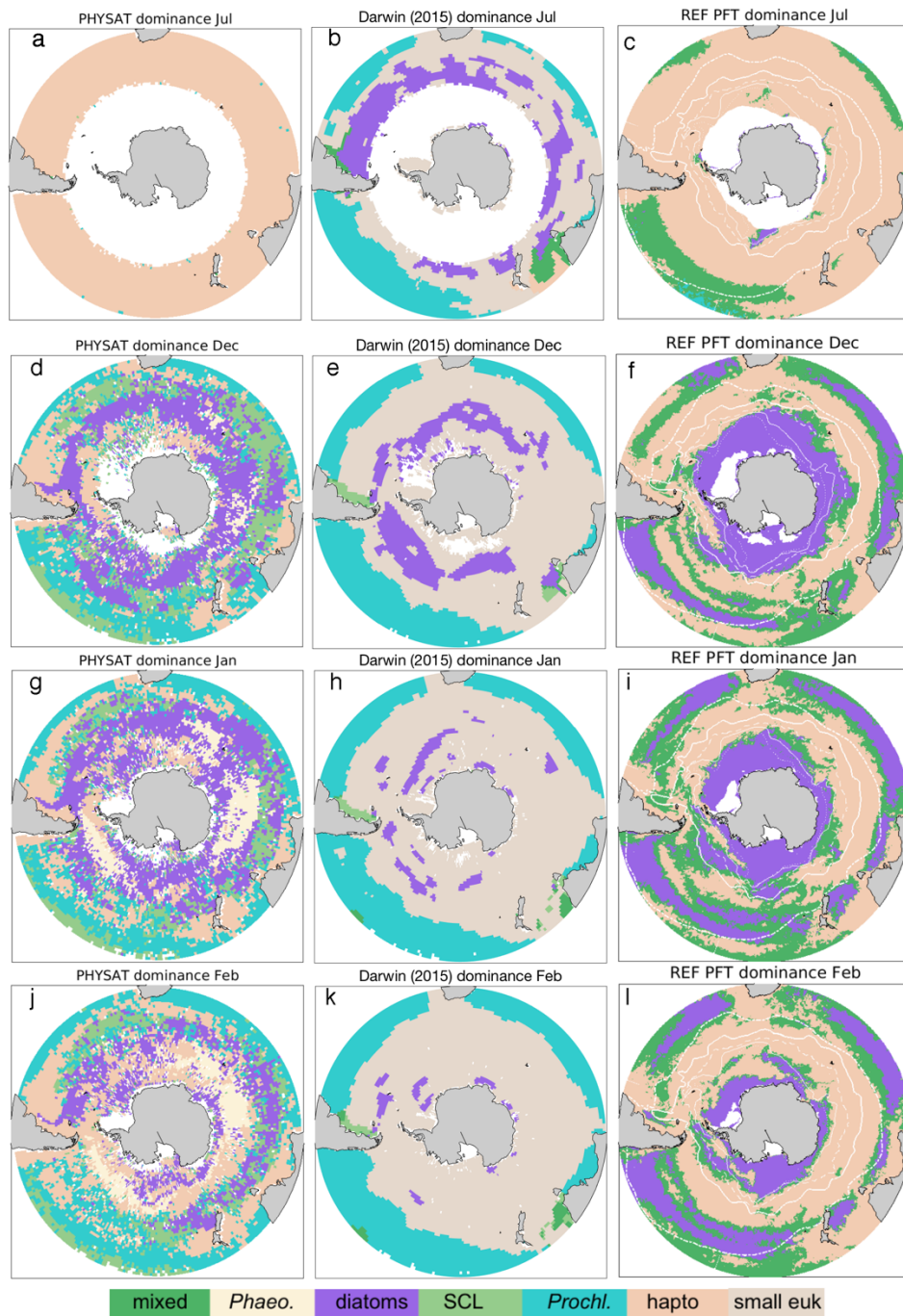


Figure 2. Climatology of surface PFT dominance retrieved by PHYSAT algorithm (1998-2006, left), simulated with the Darwin-MITgcm version of Dutkiewicz et al. (2015) (middle) and the current model set up REF (right) (2006 - 2012). "SCL" represents *Synechococcus* like prokaryotic phytoplankton (not considered in the current model version). Simulated haptophytes include coccolithophores and *Phaeocystis*. Model PFT is considered dominant if its Chla fraction of total Chla is more than 55%. The model output (REF) is masked by the area with sea ice concentration > 75% during respective month. Darwin-15 is masked by PHYSAT missing values. White contours denote the Southern Ocean fronts (Orsi et al., 1995; Orsi and Harris, 2001) as in Figure 1 **35**

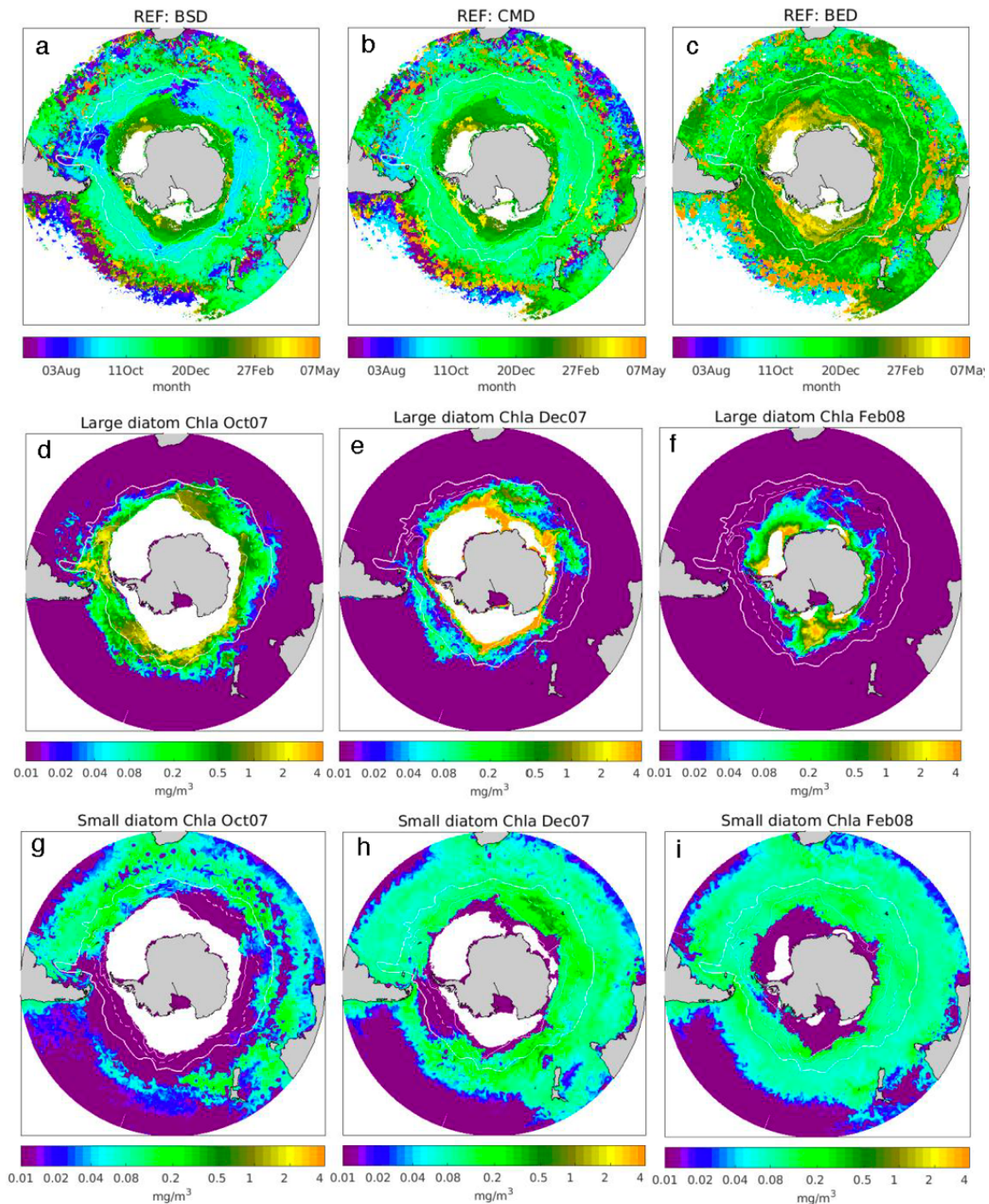


Figure 3. Upper panels - Phenological indices calculated for the REF diatom simulations over 2007/2008: a - Bloom Start Date (BSD), b - Chlorophyll-*a* Maximum Date (CMD) and c - Bloom End Date (BED). Middle and lower panels: spatial distribution of the model surface chlorophyll-*a* for large and small diatoms in the Southern Ocean for October and December 2007 and February 2008 (experiment REF). White contours denote the Southern Ocean fronts (Orsi et al., 1995; Orsi and Harris, 2001) as in Figure 1.

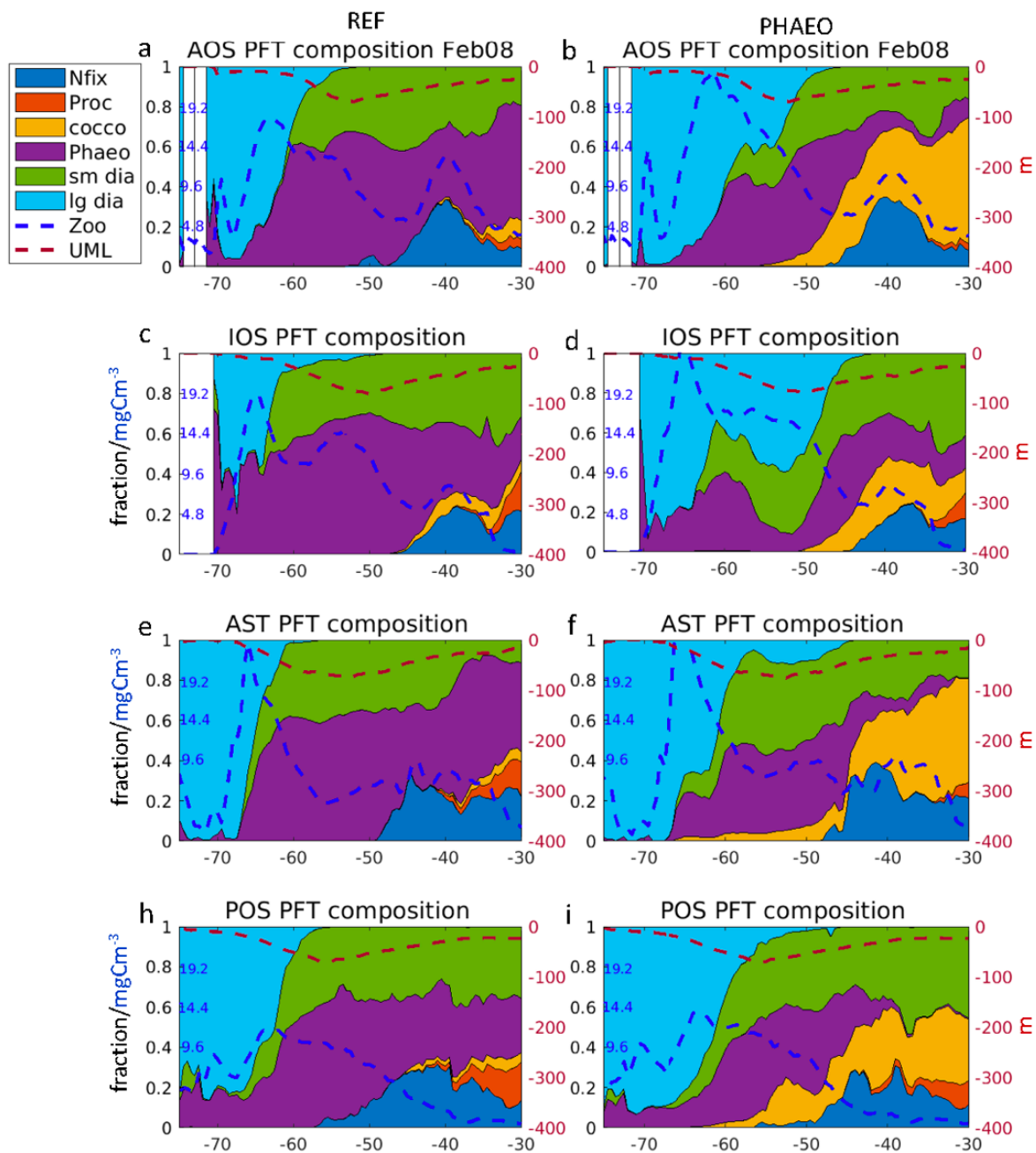


Figure 4. Meridional (from 75°S to 30°S) distribution of zonally averaged phytoplankton composition for the Atlantic Ocean sector (AOS, 60°W – 18°E), the Indian Ocean sector (IOS, 18°E – 120°E), the Australian sector (AST, 120°E – 180°E) and the Pacific Ocean sector (POS, 180°E – 60°W) in February 2008. The red dashed contour represents the upper mixed layer depth (UML, zonally averaged, m). The blue contour represents zonally averaged zooplankton concentration (mgC m^{-3}). Experiment REF (to the left); experiment PHAEO (to the right). "Cocco" for coccolithophores, "Phaeo" for "other large" (including *Phaeocystis*), "sm dia" for small diatoms and "lg dia" for large diatoms, 'Nfix' for nitrogen fixers, 'Proc' for *Prochlorococcus*.

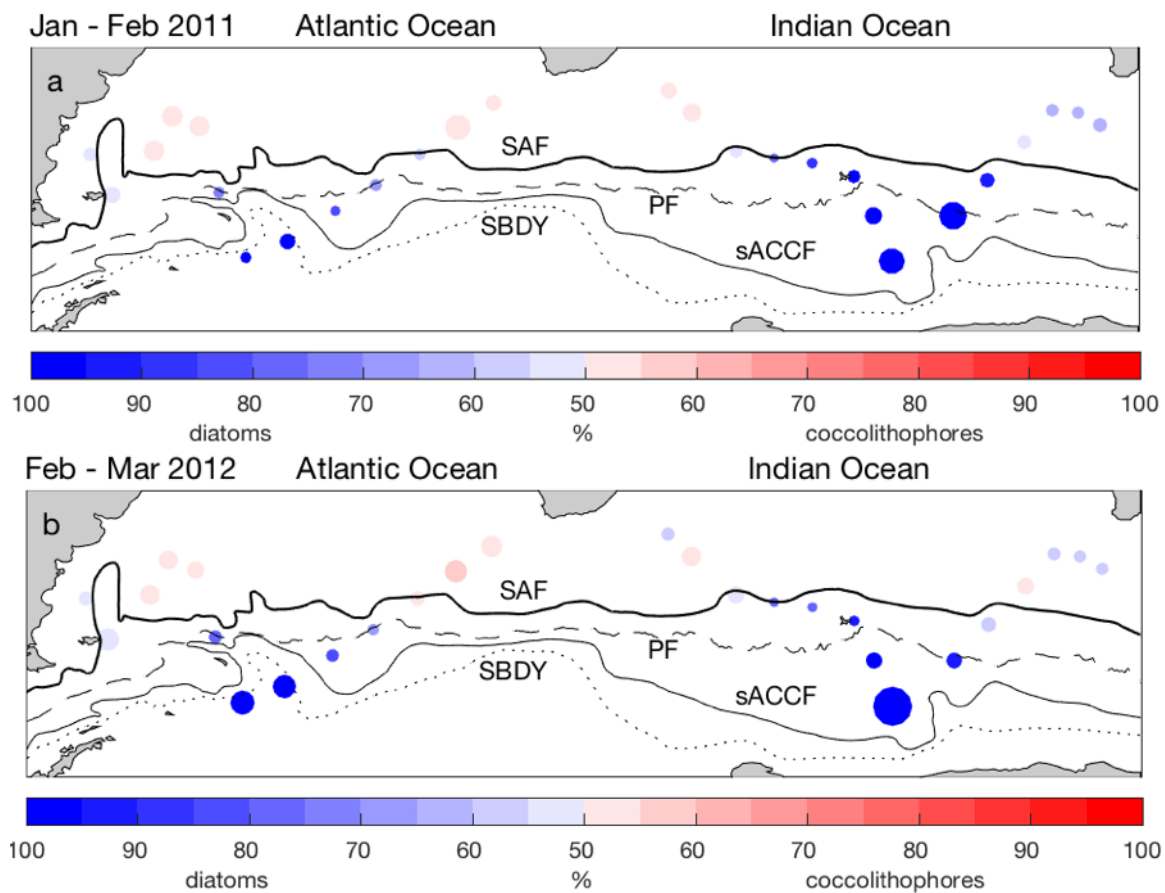


Figure 5. PHAEO diatom vs. coccolithophores dominance averaged over January - February 2011 (a) and February - March 2012 (b). The size of the circles is relative to phytoplankton carbon content (mmol C/m^3). The largest size of the circle corresponds to $3.12 (\text{mmol C/m}^3)$. Black contours denote the Southern Ocean fronts (Orsi et al., 1995; Orsi and Harris, 2001) as in Figure 1.

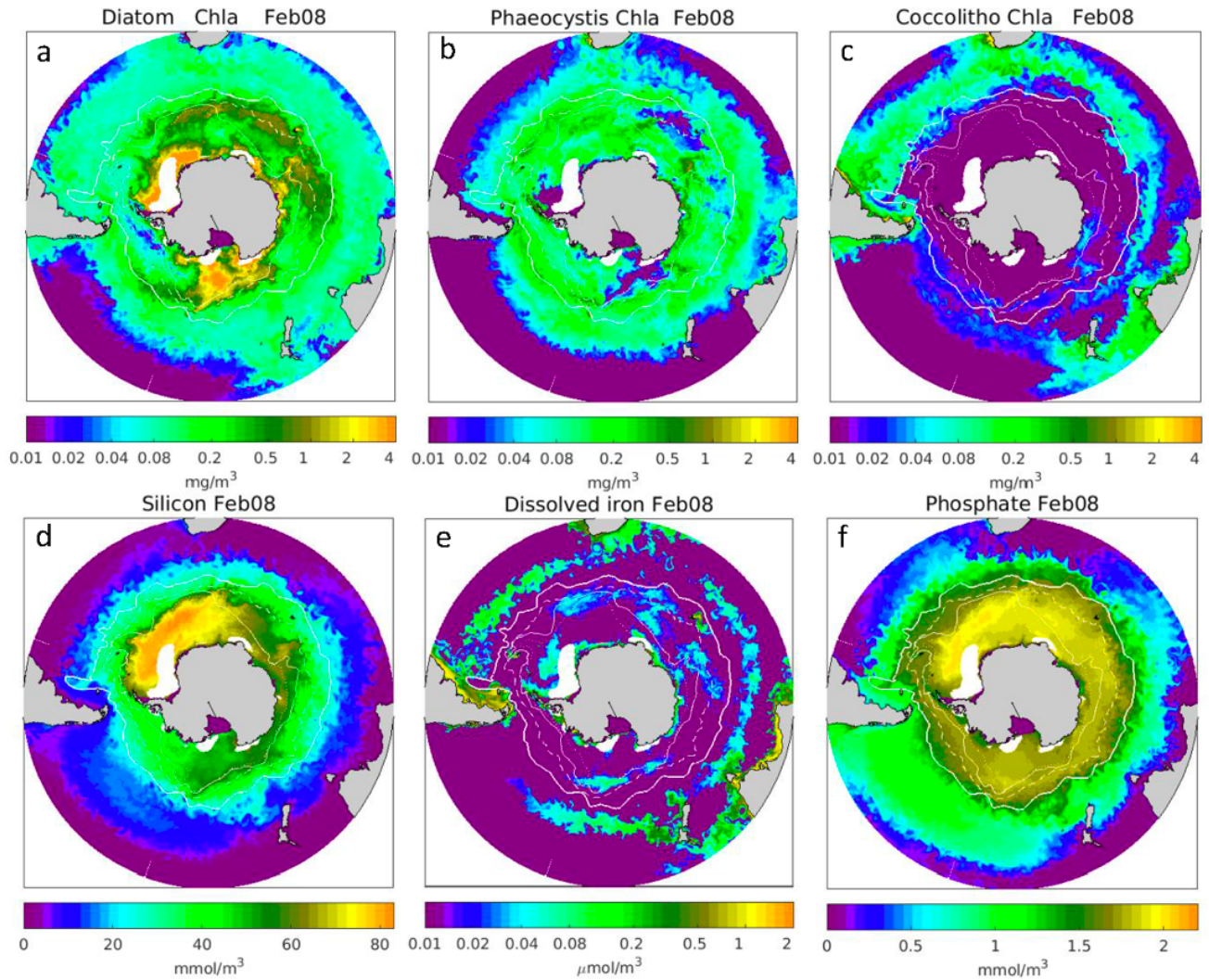


Figure 6. Surface spatial distribution of the model diatoms (a, small + large), *Phaeocystis* (b) and coccolithophores (c) Chla (mgChla m^{-3}) in the Southern Ocean for February 2008 for the experiment PHAEO. Lower panels: spatial distribution of surface silicon (d, mmol m^{-3}), dissolved iron (e, $\mu\text{mol m}^{-3}$) and phosphate (f, mmol m^{-3}) concentration for February 2008 for experiment PHAEO. White contours denote the Southern Ocean fronts (Orsi et al., 1995; Orsi and Harris, 2001) as in Figure 1.

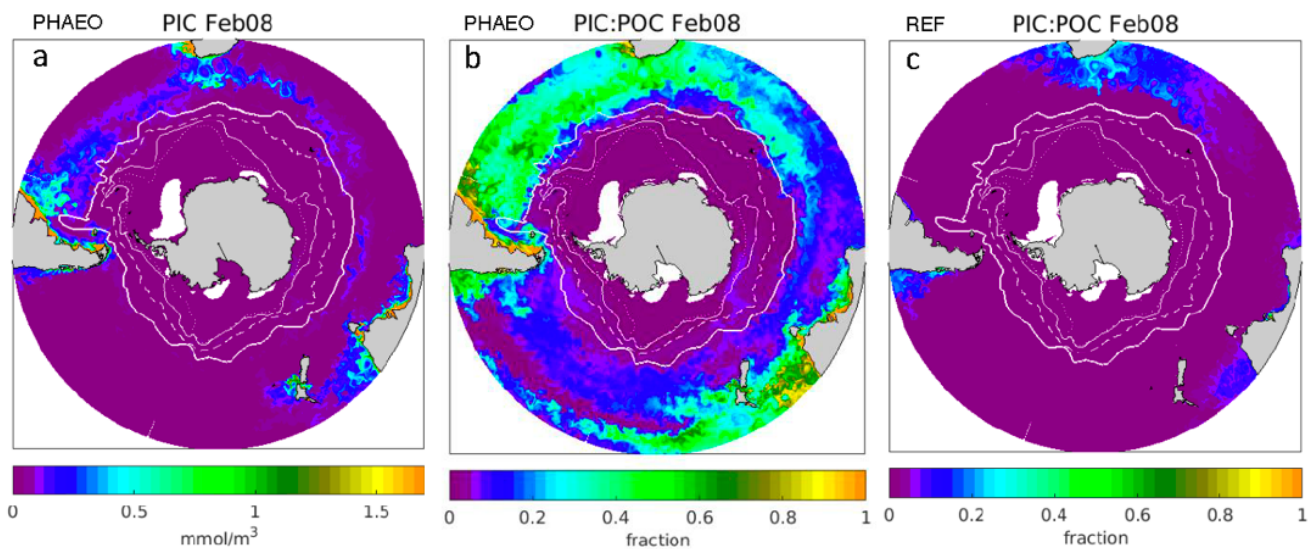


Figure 7. Spatial distribution of the model surface particulate inorganic carbon (PIC, mmol m^{-3}) for experiment PHAEO (left panel), ratio of PIC to total particulate (dead) organic carbon (PIC:POC) for experiment PHAEO (middle panel) and PIC:POC for experiment REF (right panel) in February 2008. White contours denote the Southern Ocean fronts (Orsi et al., 1995; Orsi and Harris, 2001) as in Figure 1.

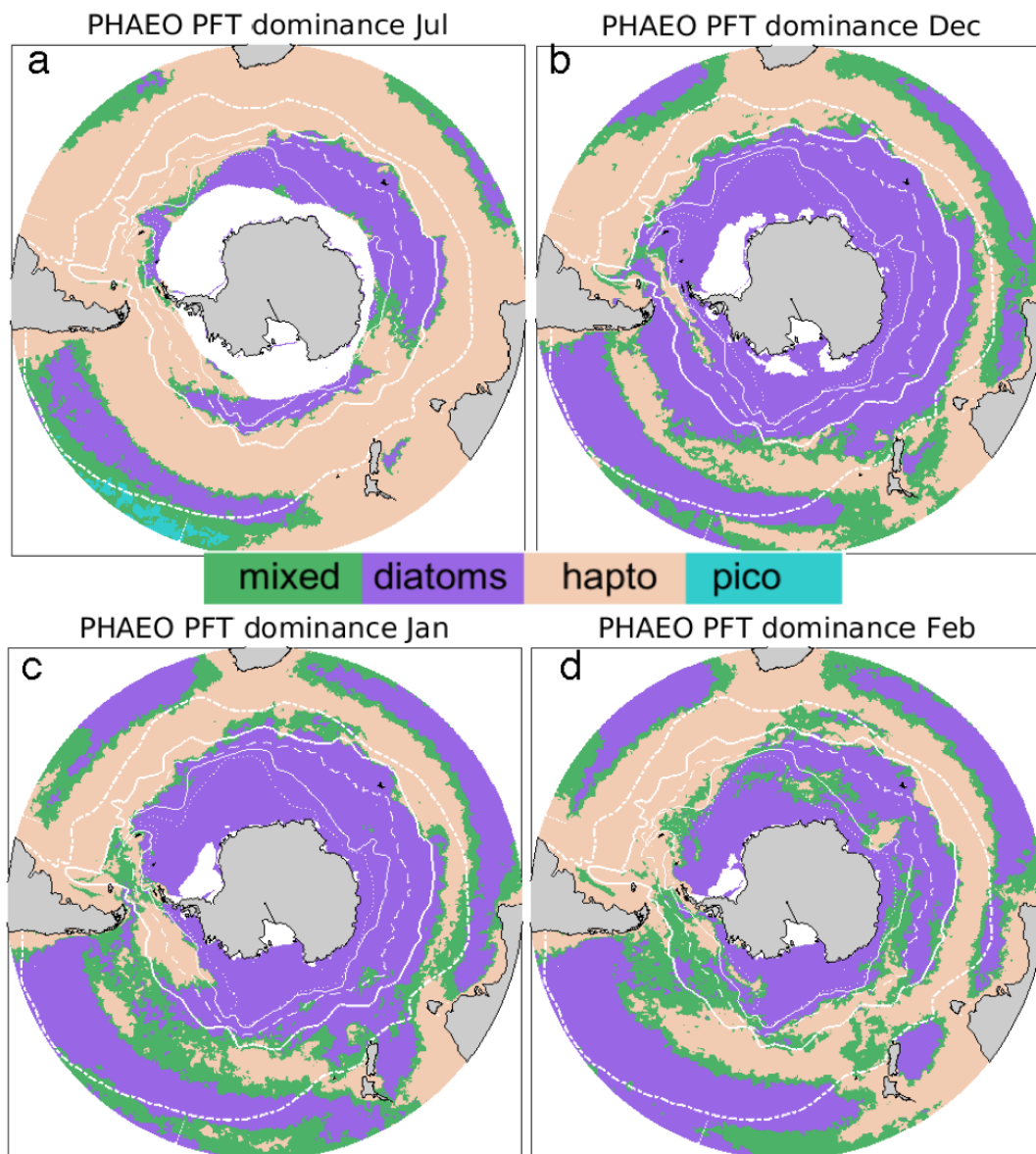


Figure 8. PHAEO climatological monthly mean surface PFT dominance for July (a), December (b), January (c), February (d) (see Figure 2 and Figures S15 and S16 for The model output is masked by the area with sea ice concentration $> 87\%$ during respective month. White contours denote the Southern Ocean fronts (Orsi et al., 1995; Orsi and Harris, 2001) as in Figure 1. The model output is masked by the area with sea ice concentration $> 75\%$ during respective month.

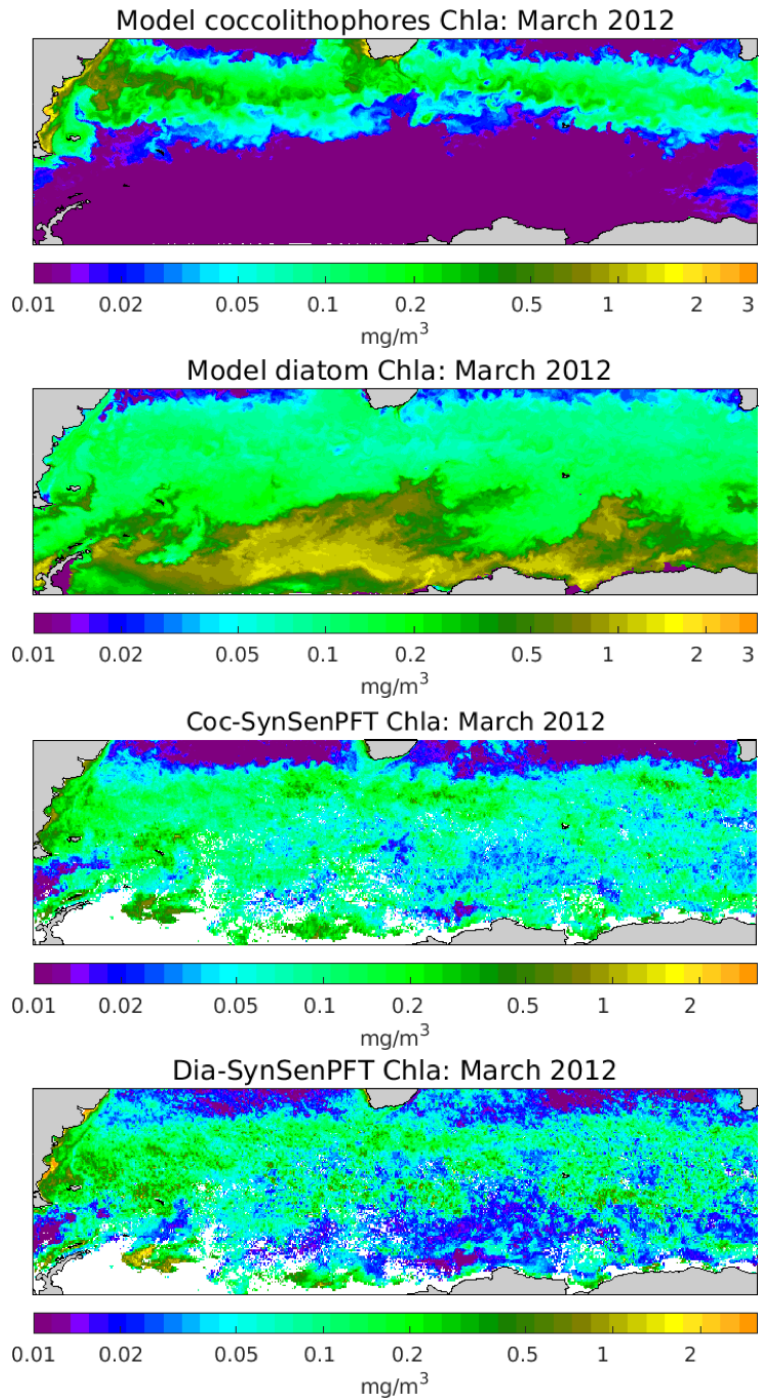


Figure 9. Surface Chla (mgChla m^{-3}) for coccolithophores and diatoms as model simulated (two upper panels, experiment PHAEO) and retrieved with SynSenPFT algorithm (two lower panels) distributed over the domain shown by Smith et al. (2017) for March 2012.